RSC Advances

ROYAL SOCIETY OF CHEMISTRY

www.rsc.org/advances

Nickel(II) and copper(II) complexes constructed with N_2S_2 hybrid benzamidine-thiosemicarbazone ligand: Synthesis, X-ray crystal structure, DFT, kinetico-catalytic and *in vitro* biological applications

Paranthaman Vijayan,[a] Periasamy Viswanathamurthi,*[a] Krishnaswamy Velmurugan,[b] Raju Nandhakumar,[b] Manickam Dakshinamoorthi Balakumaran,[c] Pudupalayam Thangavelu Kalaichelvan,[c] Jan Grzegorz Malecki[d]

[a]*Department of Chemistry, Periyar University, Salem-636 011, India.*

[b]*Department of Chemistry, Karunya University, Karunya Nagar, Coimbatore - 641 114, India.*

[c]*Centre for Advanced Studies in Botany, School of Life Sciences, University of Madras, Guindy Campus, Chennai - 600 025, Tamil Nadu, India.*

[d]*Department of Crystallography, Silsian University, Szkolna 9, 40-006 Katowice, Poland*

*To whom correspondence should be addressed, e-mail: *viswanathamurthi72@gmail.com*

Fax: +91 427 2345124

Abstract

With the aim of assessing whether transition metal complexes might be utilized as efficient biocatalysts and biological drugs, new monofunctional nickel(II) and copper(II) complexes of the types NiL (**1**) and CuL (**2**) [**H_2L** = N-(N',N'-diethylaminothiocarbonyl)benzimidoyl chloride-2-aminoacetophenone-N-methylthiosemicarbazone] were synthesized. The compounds are remarkably stable and were obtained in good yields. The structural elucidation was carried out thoroughly in both solid and solution-state by elemental analyses and various spectroscopic techniques (IR, UV-vis, ^{1}H NMR, EPR) as well as ESI mass spectrometry. The molecular structure of the compounds was investigated by single-crystal X-ray diffraction analyses. The analyses showed tetradentate coordination of ligand in nickel(II) and copper(II) complexes, in which the metal atom exhibits a square planar geometry with N_2S_2 donor fashion. Structural optimization, HOMO-LUMO energy calculation, Natural Bond Orbital (NBO) analysis of **H_2L** and its complexes **1, 2** were investigated by Density Functional Theory (DFT). The trend in binding affinities of the compounds with biomolecules such as calf thymus DNA (CT-DNA) and bovine serum albumin (BSA) protein were investigated by different spectrophotometric methods revealed an intercalative mode of interaction. Furthermore, enzyme kinetic studies reflected that the square planar complexes (**1**, **2**) are also effective in mimicking catecholase (3,5-DTBC) and phosphatase (4-NPP) like activities over parent **H_2L**. The highest k_{cat} values suggested that the selected compounds displayed higher rate of catalytic efficiency. *In vitro* cytotoxicity of the complexes on human skin cancer melanoma (A375), human cervical cancer (HeLa) and human hepatocellular carcinoma (Hep3B) cancer cell lines demonstrated that the complexes had broad-spectrum of anti-cancer activity with low IC_{50} values. The morphological assessment data obtained by acridine orange/ethidium bromide (AO/EB) and diamidino-2-phenylindole (DAPI) staining revealed that the complex **2** induces apoptosis much more effectively than **1**.

Key words: Nickel(II) and copper(II) complex, X- ray structure, DFT, DNA/BSA binding, Kinetics, MTT, Apoptosis

Introduction

Ligand design is becoming an increasingly important part of the synthetic activity in chemistry. This is of course because of the subtle control that ligands exert on the metal center to which they are coordinated.[1,2] Notably, the choice of the hybrid ligands is particularly crucial in the stabilization of highly reactive species, unusual oxidation states in promoting original reactivity[3,4] and implementing catalytic as well as biological properties.[5,6] In previous, many article have shown that mono- and bidentate ligands system may suffer from insufficient stability for *in vitro* and *in vivo* studies due to rapid ligand exchange reactions with plasma components. In common many metal(II) cores containing medium and soft donor atoms ligands were particularly recommended for *in vitro* and *in vivo* studies. Thus, chelators with a mixed sulfur and nitrogen donor sphere might be very suitable for formation of metal complexes and some of them have found in medicinal applications.[7] With above fact in mind, tetradentate N, S donor Schiff-base ligands have extensively been used as supporting ligands in d-block chemistry because of their ability to stabilize metals in different oxidation states.[8,9]

Thioureas are potentially very versatile ligands, as they are able to coordinate to a range of metal centers as either neutral ligands, monoanions, or dianions. The effectiveness of thiourea is believed to be due to the presence of lone pair of electrons in atom such as nitrogen, sulphur and oxygen and π- electron cloud that are capable of forming dative covalent bond with metals.[10] The derivatives of thiourea such as N-(dialkylaminothiocarbonyl)benzimidoyl chlorides were first synthesized and incorporated into the synthesis of corresponding benzamidines, which can readily be obtained by reactions of the benzimidoylchlorides and primary amines, with numerous metals have been broadly studied.[11] The benzamidines can be functionalized with additional donor group to modify the properties depending on the requirements. The thiosemicarbazones have been chosen to functionalize benzamidoyl chlorides due to their considerable significance with respect to their versatile coordination behavior and promising biological and pharmaceutical properties.[12-15] The new tetradentate chelator, has been synthesized from benzimidoyl chloride moiety and N-methylthiosemicarbazide (Scheme 1).

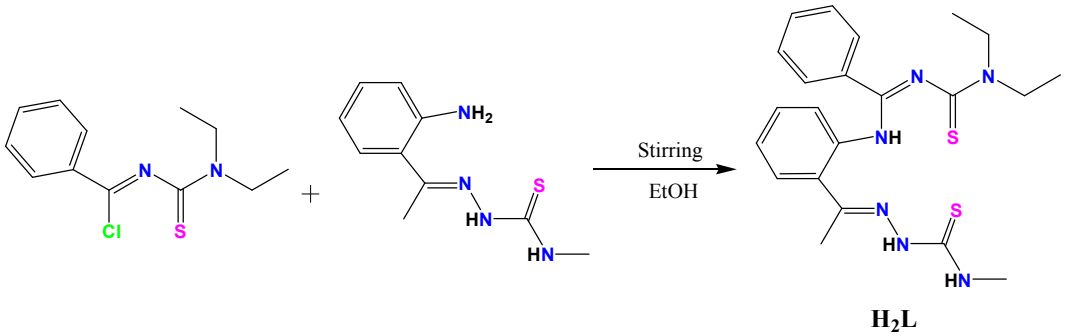

Scheme 1 Synthetic route of **H_2L** in this study

The discovery of cisplatin in 1965 was a major milestone in cancer chemotherapy, which forms a Pt-DNA adducts and ultimately inhibits cellular DNA transcription and replication. However, usage of cisplatin suffers from unprepossessing side effects such as drug resistance and severe toxicity such as nephrotoxicity and neurotoxicity.[16-18] So, the new metal based drugs with novel mechanisms of action are being developed as an alternative to platinum based drugs. Numerous Co(III), Ni(II), Cu(I/II), Zn(II) and Ru(II) complexes have been probed in quest of new developed inorganic drugs.[19a-c] Among the various metal(II) complexes, nickel and copper ions are considered as the best promising alternatives to cisplatin as anticancer drugs because its play energetic role in biological functions such as DNA, BSA, HSA and RNA interactions.[19d]

To find highly effective, target specific and less toxic drugs, much effort has been devoted to the development of metal-based anticancer agents binding to DNA through a noncovalent interaction. Three binding modes of metal complexes with DNA exist in a noncovalent way, electrostatic, groove, and intercalation. Many important applications of these complexes require that they can bind to DNA via an intercalative mode that could induce cellular degradation. The planarity of the ligand and the presence of aromatic systems are factors that favor the intercalation.[21a] Moreover, most of the recent research on clinical agents has shown that drugs (metal complexes) not only bind to the prime molecular target DNA, but also strongly interact with serum albumin proteins such as BSA and HSA.[21b] It is essential to explore drug-protein interactions as most of the drugs bound to serum albumin are usually transported as a protein complex. Attention has also been focused on the proteins that drive and control cell cycle progression.

On the other hand, the catecholase/phosphatase-like activities of some model coordination complexes have been a topic of recent interest for the development of new bioinspired catalysts.[23] Catechol oxidase is a copper-containing type-III active-site protein (Scheme 2) that catalyzes for two-electron-transfer reaction during the oxidation of a wide range of catechols known as catecholase activity, while hydrolase belong to a class of metalloenzymes that catalyzes the hydrolysis of several type of substrates including phosphate esters (4-NPP), peptides and nuclei acids.[24a] Most of the researchers have focused on dinuclear systems so far to match the original enzyme structurally where there exists a dimeric-copper active center. Recent investigations have also shown that some manganese(II/III), nickel(II), zinc(II) and cobalt(II/III) species can also mediate such catechol oxidation.[24b,c] Therefore, much attention has been focused on the catecholase/phosphatase like properties of benzamidine-thiosemicarbazone containing nickel(II) and copper(II) complexes.

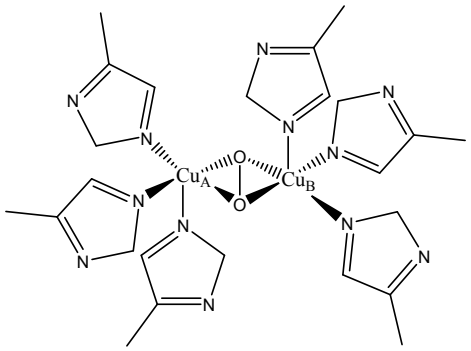

Scheme 2 Bio active dimeric copper-containing type-III protein

Therefore, through this above contribution, we reported the ligand [N-(diethylaminothiocarbonyl)]benzimidoylchloride-2-aminoacetophenone-N- methylthiosemicarba -zone] (**H_2L**) to synthesize new nickel(II) and copper(II) complexes (**1**, **2**) as shown in Scheme 3. Furthermore, the investigation of binding properties with calf thymus DNA (CT-DNA) and BSA protein on the new complexes have been carried out. Moreover **H_2L** and its complexes **1**, **2** were also investigated for possible catecholase and phosphatase like activities. In addition, cytotoxic activity of the new compounds towards normal Vero cell line, A375 (human melanoma skin cancer) human cervical cancer (HeLa) and human hepatocellular carcinoma (Hep3B) cell lines were evaluated using MTT assay along with cell death analysis by AO/EB and DAPI staining.

Results and discussion

Synthesis and characterization

The benzamidine-thiosemicarbazone ligand **H_2L** was synthesized by the reaction of N-(diethylaminothiocarbonyl)benzimidoylchloride[10] with *o*-aminoacetophenone-thiosemicarbazone[25] in presence of supporting base Et_3N. The synthesis of nickel(II) and copper(II) complexes **1**, **2** were achieved in good yields by the reaction of **H_2L** with $Ni(OAc)_2.4H_2O$ and $Cu(OAc)_2.H_2O$ respectively (Scheme 3). In this reaction, the **H_2L** acted as a dibasic tetradentate ligand with N_2S_2 fashion. The new compounds under investigation are crystalline and nonhygroscopic solids, air-stable in solution and in the solid state at room temperature, soluble in common organic solvents such as methanol, ethanol, benzene, chloroform, dichloromethane, acetone, dimethylsulfoxide, dimethylformamide and insoluble in hexane, petroleum ether and diethyl ether. The complexes have been characterized satisfactorily by elemental analyses, IR, UV-vis, ^{1}H-NMR and ESI-MS spectral studies. In addition, the molecular structure of the ligand **H_2L** and its complexes **1, 2** was confirmed by single crystal X-ray crystallography.

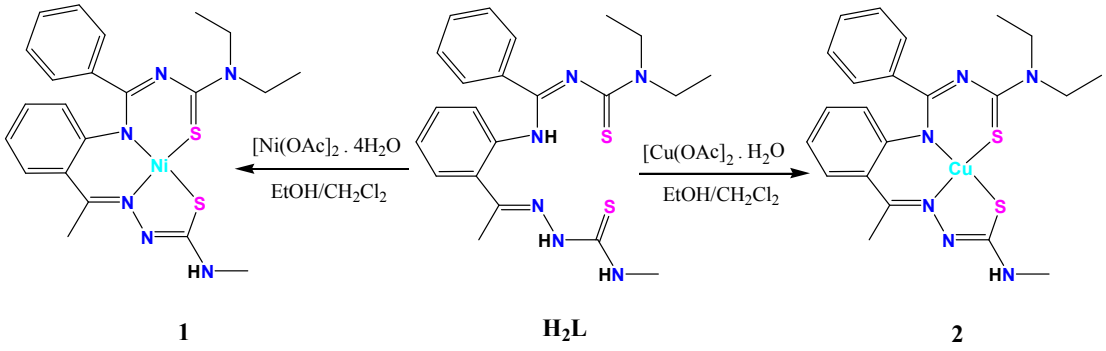

Scheme 3 Synthesis of nickel(II) (**1**) and copper(II) (**2**) complexes

IR spectroscopy has been used to confirm the deprotonation and exact binding mode of the ligand. In the IR spectrum of the ligand, there are three ν_{NH} bands were observed in the range of 3236-3302 cm^{-1}.[26] On complexation, two ν_{NH} peaks disappeared from the spectra of complexes indicate the deprotonation of these groups in the ligand and a sharp band at 3390-3417 cm^{-1} was assigned to the ν_{NH} stretch of the H_3C-NH-C-S group. A strong vibration

observed at 1668-1717 cm^{-1} in the spectrum of ligand corresponding to $\nu_{C=N}$ groups which were shifted to lower frequency in the complexes. A sharp band at 838 cm^{-1} was attributed to $\nu_{C=S}$ group of diethylaminothiocarbonyl moiety in the H_2L. This was shifted to lower frequencies region at 784-790 cm^{-1} in the complexes indicates the participation of sulphur in the coordination. Furthermore, the one more band at 781 cm^{-1} was assigned to $\nu_{C=S}$ group present in the thiosemicarbazone part of H_2L, which was completely disappeared in the spectra of complexes and new band appeared around 761-764 cm^{-1} was assigned to ν_{C-S} indicates the thione-thiol tautomerism of –NH–C=S group and subsequent coordination of thiolate sulfur after deprotonation. These clearly confirm the coordination occurs through nitrogen and sulphur atoms.

The clearest characterization of the synthesized compounds that can be seen from the ^{1}H-NMR spectra of ligand **H_2L** and its complex **1.** The datas are summarized in the experimental section and the resulting spectra are depicted as Fig. S1, S2. In the ^{1}H NMR spectra, the signal due to the –NH hydrazinic group of ligand appeared at 12.72 ppm which was absent in complex supporting the ketoenolization and coordination of thiolate sulphur.[27] The signal due to the C_{ar}-NH group appeared at 8.47 ppm in the spectrum of **H_2L** has completely disappeared in the spectrum of complex indicates deprotonation upon complex formation. The signal appeared at 8.10 ppm was attributed to NH-CH_3 group of **H_2L,** which was shifted to a high field region at 4.85 ppm even after complexation.[28] However, the proton signals of the two methylene groups in **H_2L** and its complex **1**, which should consequently be two quartets, appear as four well separated multiplet resonances at 3.74-4.12 ppm.[6] This results in magnetic nonequivalence with respect to their axial and equatorial positions of four methylene protons as indicated by four separated signals with ABX_3 splitting patterns as previously reported.[29] Furthermore two triplet signals region at 1.22-1.33 ppm for the methyl groups in $N(CH_2CH_3)_2$ are observed in the spectra of **H_2L** and its complex **1**.[7] In addition, the spectra of **H_2L** and its complex **1** showed a series of overlapping multiplets for aromatic protons at 6.40-7.54 ppm.

The UV–vis spectra of the complexes have been recorded in DMSO solution (0-48 h) (Figure S3) are similar, suggesting that the complexes retain their structure in solution within the timeframe used for the biological experiments. Electronic spectra of the compounds displayed intense absorptions in the visible and ultraviolet regions. The absorptions in the ultraviolet region

are assignable to transitions within the ligand orbitals. The bands around 236-298 nm were assigned to ligand-centred (LC) $\pi\rightarrow\pi^*$ and $n\rightarrow\pi^*$ transitions.[15a] The lowest energy absorption maxima located in the 367-374 nm range may be assigned to an S(pπ)→M(dπ) ($M = Ni^{2+}$, Cu^{2+}) LMCT transition caused by the promotion of the electron from the full HOMO of the ligand of primarily sulfur pπ character to the empty LUMO of metal ion dπ character. Furthermore, the complexes showed a broad bands at 431-491 nm region, which is attributed to the d-d transitions bands of spin-paired d^8 (complex **1**) and d^9 (complex **2**) species with a square-planar structure (Fig. S3). The geometry of the complexes further confirmed by single crystal X-ray diffraction analyses.

The EPR spectrum measured at 9.45 GHz (X-band) of the complex **2** correspond to an axial g-tensor showing broad signals (Fig. S4). The g-parameters, $g_{\|}$ and $g_{\perp}$, were determined for the complex **2,** but no coupling parameters could be extracted. The averaged g-values (g_{av}) were obtained through the relationship between the anisotropic parameter of the g-tensor, from the following expression $g_{av} = (g_{\|} + 2\times g_{\perp})/3$. The complex **2** exhibits an anisotropic spectra with $g_{\|}$ = 2.078, $g_{\perp}$ = 2.031 and g_{av} = 2.046 which is consistent with the presence of a square planer geometry as evident from the crystal structure of **2.** These parameters are in good agreement with that of the related square planar Cu^{2+} systems and are typical of axially symmetrical d^9 copper(II) complexes[15b] (Fig. S4).

The ESI-MS analyses of **H_2L** and its complexes **1**, **2** shows the most abundant peaks at m/z, 441.55, 498.42, 503.52 respectively which were assigned to $[M + H]^+$ ions. The obtained molecular masses are in good agreement with that of the calculated molecular masses (Fig. S5-S7).

Single crystal X-ray diffraction studies

Single-crystal X-ray diffraction studies of compounds (**H_2L**, **1** and **2**) confirm the conclusions drawn from the spectroscopic studies. To gain insight into the coordination chemistry and structural parameters of these compounds, single crystals were isolated as good quality by slow evaporation of a concentrated ethanol/dichloromethane solution and characterized by X-ray diffraction. Details of the data collection, solution and refinement are gathered in the experimental section and Table 1. The ORTEP view of the molecular structure of

compounds along with a partial atom numbering scheme is shown in Figure 1-3 and important bond lengths and angles for the compounds are summarized in Table 2.

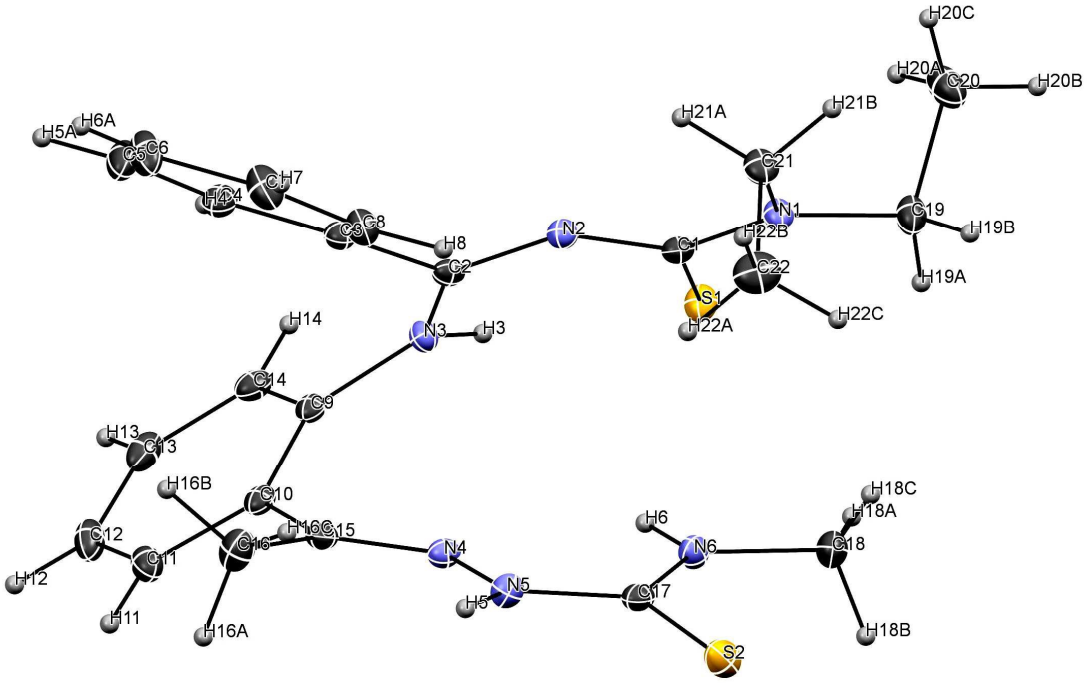

Fig. 1 Perspective view (25% probability ellipsoids) of **H_2L** with the atom numbering scheme.

Figure 1 depicts the molecular structure of **H_2L**. The **H_2L** crystallized in the triclinic *P*i space group. Selected bond lengths and angles are summarized in Table 2. The protonation of the nitrogen atoms N3 and N5 is experimentally justified by the detection of peaks of electron density in the final Fourier map, which can be assigned to corresponding hydrogen atoms are involved intermolecular hydrogen bonding. The N(3)-H(3)-S(1) hydrogen bond forms the intramolecular ring of $S_1^1(6)$ type. The C–N and C=N bond distances (see Table 2) found in **H_2L** agree well with that reported for similar other ligands containing C–N/C=N bonds. The thione form is confirmed by the bond length of C(1)-S(1) (1.704 Å), C(17)-S(2) (1.674 Å) which are very close to a formal C=S bond length (1.60 Å). Examination of packing diagram of **H_2L** revealed that in the structure exhibit intermolecular π-π stacking interaction between the parallel C(9)-C(14) ring and its equivalent obtained by (-x, 1-y, -z) symmetry transformation although the geometrical parameters with distance of 3.575 Å and shift equal to 1.440 Å indicate rather weak interaction as shown in Fig S8.

Table 1 Crystal data and structure refinement for ligand **H_2L** and its complexes **1**, **2**

	H_2L	**1**	**2**
Empirical formula	C_{22} H_{28} N_6 S_2	C_{22} H_{26} N_6 Ni S_2	C_{22} H_{26} Cu N_6 S_2
Formula weight	440.62	497.32	502.15
Temperature (K)	100(2) K	295(2) K	295(2)
Wavelength (Å)	0.71073 Å	0.71073 Å	0.71073 Å
Crystal system	Triclinic	orthorhombic	orthorhombic
Space group	*P*ī	*P*bca	*P*bca
Unit cell dimensions			
a (Å)	7.831(6) Å	13.2007(7) Å	13.3637(4)
b (Å)	10.956(8) Å	17.5298(9) Å	17.6802(7)
c (Å)	14.357(18) Å	20.1722(11) Å	19.9696(6)
α (°)	75.594(18)°	90°	90°
β (°)	89.60(3)°	90°	90°
γ (°)	72.16(2)°	90°	90°
Volume ($Å^3$)	1132.47(5) $Å^3$	4668.0(4)$Å^3$	4718.3(3)$Å^3$
Z	2	8	8
Density (calcd) MgM^{-3}	1.292 Mg/m^3	1.415 Mg/m^3	1.414 Mg/m^3
Absorption coefficient	2.291 mm^{-1}	1.032 mm^{-1}	1.124 mm^{-1}
F(000)	468	2080	2088
Crystal size (mm^3)	0.12 x 0.07 x 0.03	0.37 x 0.17 x 0.03	0.25 x 0.22 x 0.17
Theta range for data collection	3.18 to 73.12°	3.44 to 25.04°	3.608 to 25.07°
Index ranges	-9<=h<=8, -13<=k<=12 -17<=l<=17	-15<=h<=15 -20<=k<=20 -19<=l<=24	-15<=h<=11 -21<=k<=14 -23<=l<=19
Reflections collected	12690	16086	13366
Independent reflections	4299 [R(int) = 0.0182]	4122 [R(int) = 0.0666]	4158 [R(int) = 0.0314]
Data/restraints/parameters	4299 / 0 / 275	4122 / 0 / 284	4158 / 0 / 284
Goodness-of-fit on F^2	1.132	1.059	1.049
Final R indices [I>2sigma(I)]	R1= 0.0360, wR2= 0.1007	R1= 0.0440, wR2= 0.1096	R1= 0.0372, wR2= 0.0910
R indices (all data)	R1= 0.0364, wR2 = 0.1011	R1= 0.0607, wR2 = 0.1180	R1= 0.0511, wR2= 0.0968

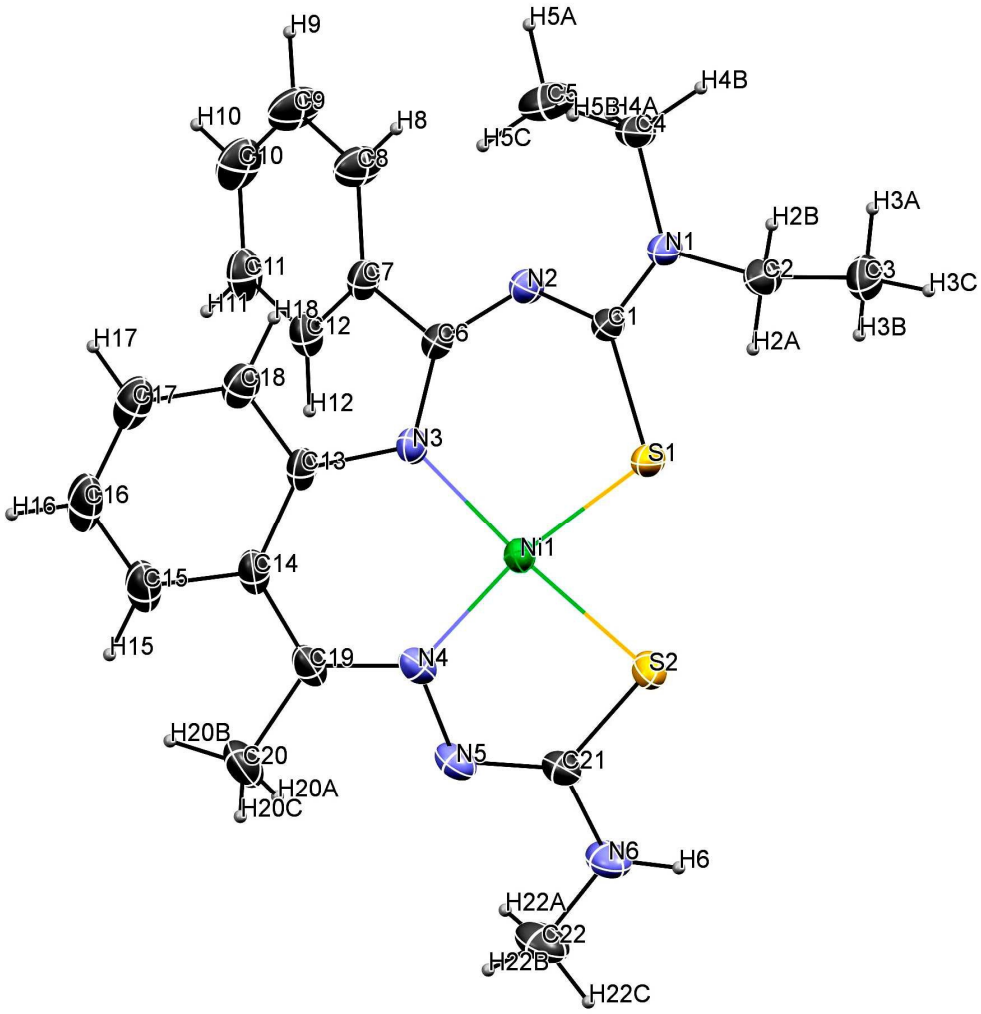

Fig. 2 Perspective view (25% probability ellipsoids) of complex **1** with the atom numbering scheme.

Table 2 Selected bond lengths (Å) and bond angles (°) for **H_2L** and its complexes **1**, **2** with the optimized geometrical values

H_2L	X-ray	DFT	**1**	X-ray	DFT	**2**	X-ray	DFT
C(1)-N(1)	1.339(2)	1.358	N(3)-Ni(1)	1.872(2)	1.890	N(3)-Cu(1)	1.932(2)	1.954
C(1)-S(1)	1.704(2)	1.784	S(1)-Ni(1)	2.149(9)	2.262	S(1)- Cu(1)	2.244(7)	2.365
C(1)-N(2)	1.362(2)	1.371	N(4)-Ni(1)	1.900(2)	1.911	N(4)- Cu(1)	1.981(2)	1.997
C(2)-N(2)	1.309(2)	1.325	S(2)-Ni(1)	2.157(9)	2.276	S(2)- Cu(1)	2.230(9)	2.361
C(2)-N(3)	1.333(3)	1.356	N(3)-C(6)	1.353(3)	1.354	N(3)-C(2)	1.353(3)	1.367
C(9)-N(3)	1.418(2)	1.428	N(3)-C(13)	1.409(3)	1.419	N(3)-C(9)	1.400(3)	1.412
C(15)-N(4)	1.274(2)	1.301	N(4)-C(19)	1.319(4)	1.315	N(4)-C(15)	1.308(4)	1.314
C(17)-N(5)	1.354(2)	1.386	S(2)-C(21)	1.729(3)	1.805	S(2)-C(17)	1.739(3)	1.808
C(17)-N(6)	1.323(2)	1.338	S(1)-C(1)	1.717(3)	1.789	S(1)-C(1)	1.720(3)	1.789
C(17)-S(2)	1.674(2)	1.730	N(2)-C(6)	1.306(4)	1.339	N(2)-C(2)	1.308(3)	1.335
N(1)-C(1)-S(1)	120.5(1)	120.1	N(3)-Ni(1)-N(4)	93.5(1)	92.0	N(3)-Cu(1)-N(4)	92.22(9)	91.9
C(2)-N(3)-H(3)	116.3(1)	113.2	N(4)-Ni(1)-S(2)	87.48(2)	86.7	N(4)-Cu(1)-S(2)	86.67(7)	85.7
C(15)-N(4)-N(5)	118.5(1)	119.6	S(2)-Ni(1)-S(1)	85.65(3)	88.9	S(2)-Cu(1)-S(1)	89.58(3)	90.5
N(6)-C(17)-S(2)	122.8(1)	125.7	N(3)-Ni(1)-S(1)	95.32(7)	92.4	N(3)-Cu(1)-S(1)	94.83(7)	92.4
N(5)-C(17)-S(2)	120.6(1)	118.5	N(3)-Ni(1)-S(2)	168.47(8)	173.0	N(3)-Cu(1)-S(2)	166.17(7)	169.8
C(9)-N(3)-H(3)	116.3(1)	116.6	N(4)-Ni(1)-S(1)	167.35(8)	175.3	N(4)-Cu(1)-S(1)	164.80(7)	174.2

Table 3 Hydrogen bonds for the **H_2L** and its complexes **1**, **2** [Å and °]

Compound	D–H….A	d(D–H)	d(H…A)	d(D….A)	<(DHA)
H_2L	N(3)-H(3)-S(1)	0.86	2.28	2.968(2)	137.2
	N(5)-H(5)-S(2)	0.86	2.61	3.351(2)	145.2
	N(6)-H(6)-N(4)	0.86	2.19	2.577(2)	106.9
1	C(2)-H(2A)-S(1)	0.97	2.57	2.963(3)	104.3
	C(20)-H(20A)-N(5)	0.96	2.24	2.600(5)	101.2
2	C(16)-H(16B)-N(5)	0.96	2.21	2.611(4)	103.9
	C(19)-H(19B)-S(1)	0.97	2.56	2.949(3)	104.2

Symmetry operation: H_2L: : 'x, y, z'; '-x, -y, -z', Complex **1**: 'x, y, z"-x+1/2, -y, z+1/2"x+1/2,-y+1/2,-z"-x, y+1/2, -z+1/2"-x, -y, -z"x-1/2, y, -z-1/2"-x-1/2, y-1/2,z"x, -y-1/2, z-1/2', Complex **2**: 'x, y, z"-x+1/2, -y, z+1/2"x+1/2,-y+1/2,-z"-x, y+1/2, -z+1/2"-x, -y, -z"x-1/2, y, -z-1/2"-x-1/2, y-1/2,z"x, -y-1/2, z-1/2'. [D= donator, A=acceptor]

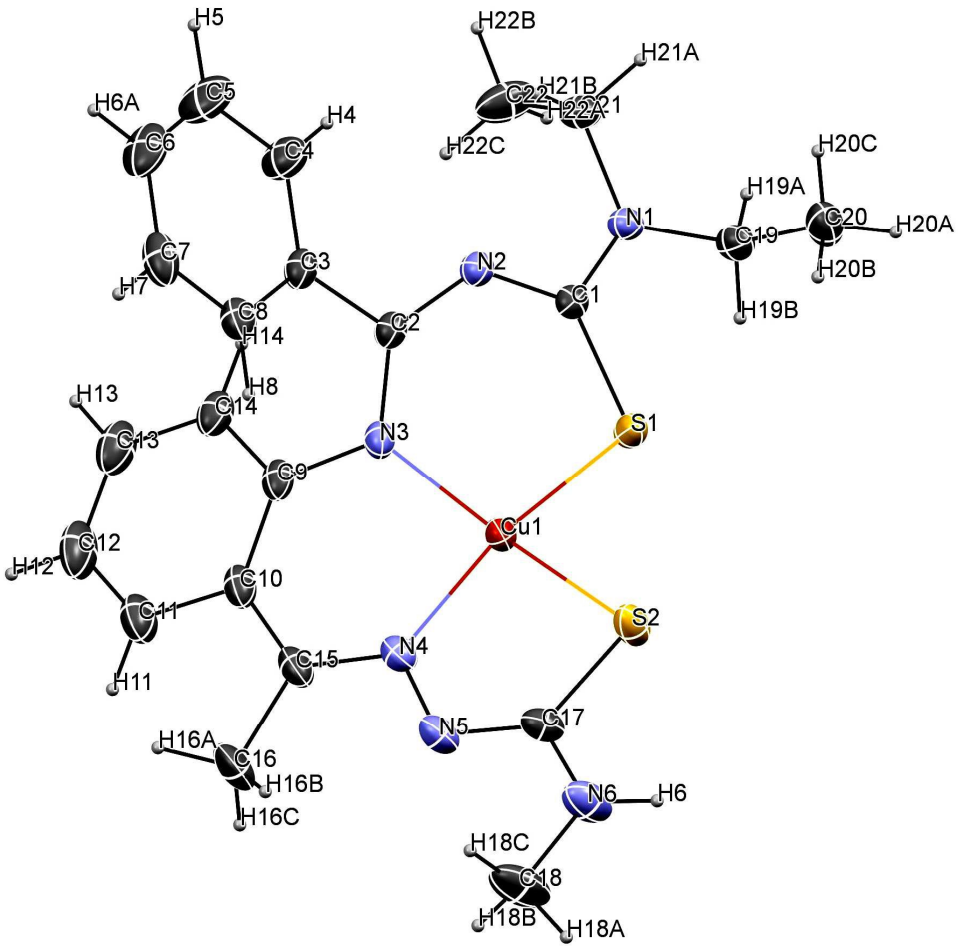

Fig. 3 Perspective view (25% probability ellipsoids) of complex **2** with the atom numbering scheme.

A perspective view of the complexes **1** and **2** with the atomic numbering scheme is depicted in Fig. 2, 3, while selected bond lengths and angles are given in Table 2. The complexes **1**, **2** crystallized in the triclinic belonging to the *P*bca space group. The metal ion adopted a square planer geometry with bonding of the **H_2L** as dibasic tetradentate (SNNS) donors. The *trans* angles are N(3)-Ni(1)-S(2), 168.47(8)^o and N(4)-Ni(1)-S(1), 167.35(8)^o (for **1**) and N(3)-Cu(1)-S(2), 166.17(7)^o and N(4)-Cu(1)-S(1), 164.80(7)^o (for **2**) which showed a deviation from the expected linear *trans* geometry, suggesting distortion in the square-planar coordination geometry. The metal bond distances Ni-N, Ni-S in complex **1** and Cu-N, Cu-S in complex **2** (Table 2) are well agree with reported nickel(II) and copper(II) complexes.[31a,b] Furthermore,

there exists intermolecular hydrogen bonding between the the atom (C–H···N/S contact) of the **H_2L** and its complexes **1**, **2** showed in Table 3. The unit cell packing diagram of compounds along with hydrogen bonding is given in Fig. S9.

Theoretical calculations

HOMO and LUMO are referred to as frontier orbitals. The energy difference between the HOMO and LUMO is termed as HOMO–LUMO energy gap. The difference in energy between two frontier orbitals can be used to predict the strength and stability of transition metal complexes as well as the colors they produce in solution. The calculations using the density functional theory (DFT) method of GAUSSIAN-09 were carried out to electronic structure of compounds. A molecule with a small gap is more polarized and is known as soft molecule.[32] The lowering of the HOMO-LUMO band gap is essentially a consequence of the large stabilization of the LUMO due to the strong electron-accepting ability of the electron-acceptor group.

The molecular structure of the **H_2L** and its complexes **1**, **2** the deprotonated forms were characterized through computational studies in a solid phase. Contour plots of frontier molecular orbitals of the complexes and the energy gap was also calculated (Fig. 4). Positive and negative regions are shown in red and blue colors respectively, and the geometrical parameters have already been given in Table 1. In general, there is a good correlation between the optimized structures and X-ray crystal structures of **H_2L** and its complexes **1**, **2**. The perfect square planer geometries of the complexes are also reflected in their calculated structures. It is seen that the complexes, the electron density of the HOMO is localized largely on the metal ion surrounding (N, S atom) only and to a very smaller extent from the ligand, while in the LUMO major contributions from ligand and to a lesser extent from the metal ion surrounding without relevant contributions. So the electron transfer occurs from the highest occupied molecular orbital (HOMO) to the lowest unoccupied molecular orbital (LUMO). It can be inferred that the electron transfer in complexes is related to LMCT. The calculated HOMO energies of the complexes vary as **H_2L** (-5.68 eV) < **1** (-5.25 eV) < **2** (-5.31 eV) and those of LUMO exhibit a similar trend: **H_2L** (-2.04 eV) < **1** (-2.15 eV) < **2** (-2.05 eV). The HOMO–LUMO energy gaps in compound **H_2L** (3.64 eV), complex **1** (-3.12 eV) and **2** (-3.20 eV) are almost the small different, which is consistent with the experimentally observed order of biological efficiencies of complexes. The

calculated atomic charge, electronic configuration of donor atoms and metal centered atoms are listed in Table 4.

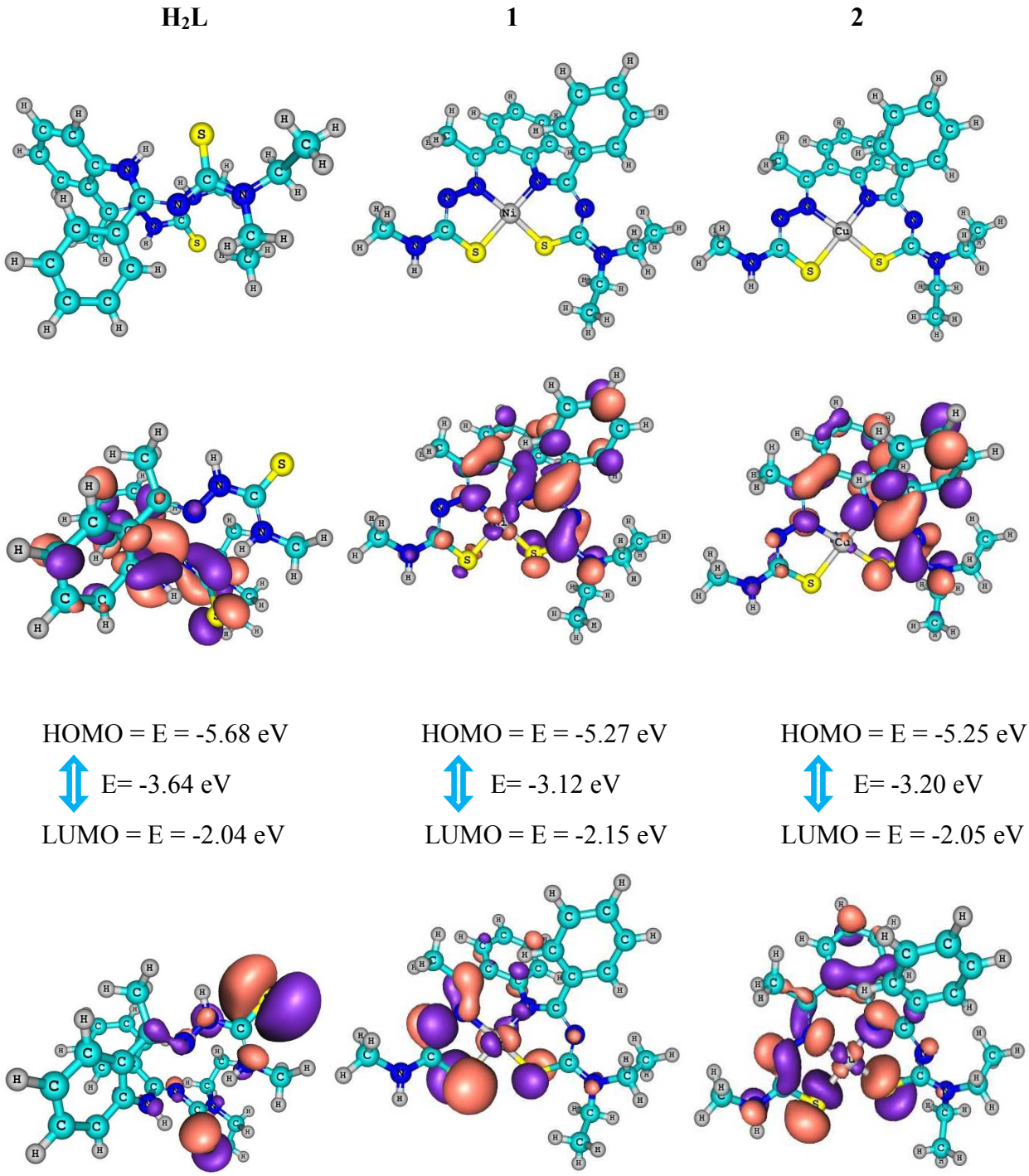

Fig. 4 Frontier molecular orbitals of compounds and their HOMO-LUMO energy gap and B3LYP/6-311G ground state optimized geometry of compounds (top).

Table 4 Charges (a.u.) and electron configurations of atoms for complexes **1, 2**

	Complex **1**		Complex **2**	
Atom	Charge (eV)	Electronic configuration	Charge (eV)	Electronic configuration
Ni/Cu	0.95397	[core]4S(0.41)3d(8.60)4p(0.02) 5S(0.02)	1.19451	[core]4S(0.43)3d(9.35)4p(0.01)5S (0.01)
N1(6)	-0.65053	[core]2S(1.32)2p(4.31)3p(0.01)	-0.72124	[core]2S(1.33)2p(4.37) 3p(0.01)
N2(7)	-0.37386	[core]2S(1.35)2p(4.00) 3p(0.02)	-0.42138	[core]2S(1.36)2p(4.04) 3p(0.02)
S1(2)	-0.28649	[core]3S(1.80)3p(4.47)4S(0.01) 4p(0.01)	-0.34276	[core]3S(1.81)3p(4.52)4S(0.01) 4p (0.01)
S2(3)	-0.36154	[core]3S(1.81)3p(4.53)4p(0.01)	-0.42362	[core]3S(1.82)3p(4.58)4S(0.01) 4p(0.01)
C1(11)	0.34264	[core]2S(0.86)2p(2.77)3p(0.02)	0.34451	[core]2S(0.86)2p(2.77)3p(0.02)
C2(39)	0.31027	[core]2S(0.86)2p(2.79)3S(0.01) 3p(0.03)	0.30966	[core]2S(0.87)2p(2.79)3S(0.01)3p (0.03)

From the assumption of the Table 4, the electron populations on s and p orbitals of nitrogen and sulfur donor atoms in both complexes are less than the expected values of valence orbitals, while the computed electron population in the central ion in both complex **1**, **2** is more than the expected value in M^{2+} (Ni, Cu) with d^8, d^9 electronic configuration respectively.[33] The calculated formal charge on the metal ion (**1** = 0.954 eV; **2** = 1.195 eV) in the complexes was lower than the formal charge +2, confirming a significant charge donation from the ligand **H_2L**. This confirms the electron transmission of donor atoms toward the central metal. The calculated electronic configurations (Table 4) of the donor atoms with reference to s and p orbitals are consistent with electron donation towards the metal ion.

DNA interaction studies

Stability of compounds

Before to carry out DNA binding studies, the stability of the complex is paramount for its application. The stability of the selected compounds (**H_2L**, **1** and **2**) has been detected in Tris-HCl buffer (5 mM Tris-HCl-50 mM NaCl buffer, pH = 7.2) at four different time points (0 min, 1 hr, 6 hr and 12 hr) through the UV absorption method. The UV-vis spectral results did not reveal any appreciable change in either the intensity or the position of the

absorption bands in Tris-HCl buffer solution (Fig. S3). This demonstrates that the compounds keep a stable structure under physiological conditions.

Fluorescence emission titration

DNA is often a vital target to mediate the targeted apoptosis or necrosis to the cells replication. So the binding affinity of the metal complexes to CT-DNA was used as primary studies for chemotherapeutic agents. These studies were carried out different spectral methods. Considered as a basic testing method, fluorescence spectroscopy is one of the most commonly used techniques for exploring the interaction of any drug with CT-DNA.[34] This technique is commonly used to study the binding mode (and their likely nature) between DNA and metal complexes. The emissive titration studies have been performed by monitoring the changes in emission intensity by aliquot addition of DNA. Usually, intercalation mode of interaction between the metal complexes and DNA results in hypochromism with or without red/blue shift; on the other hand, non-intercalative/electrostatic interaction causes hyperchromism. Therefore, typical emissive titration curves for the selected compounds in the absence and presence of CT-DNA at different increasing concentrations were implemented.

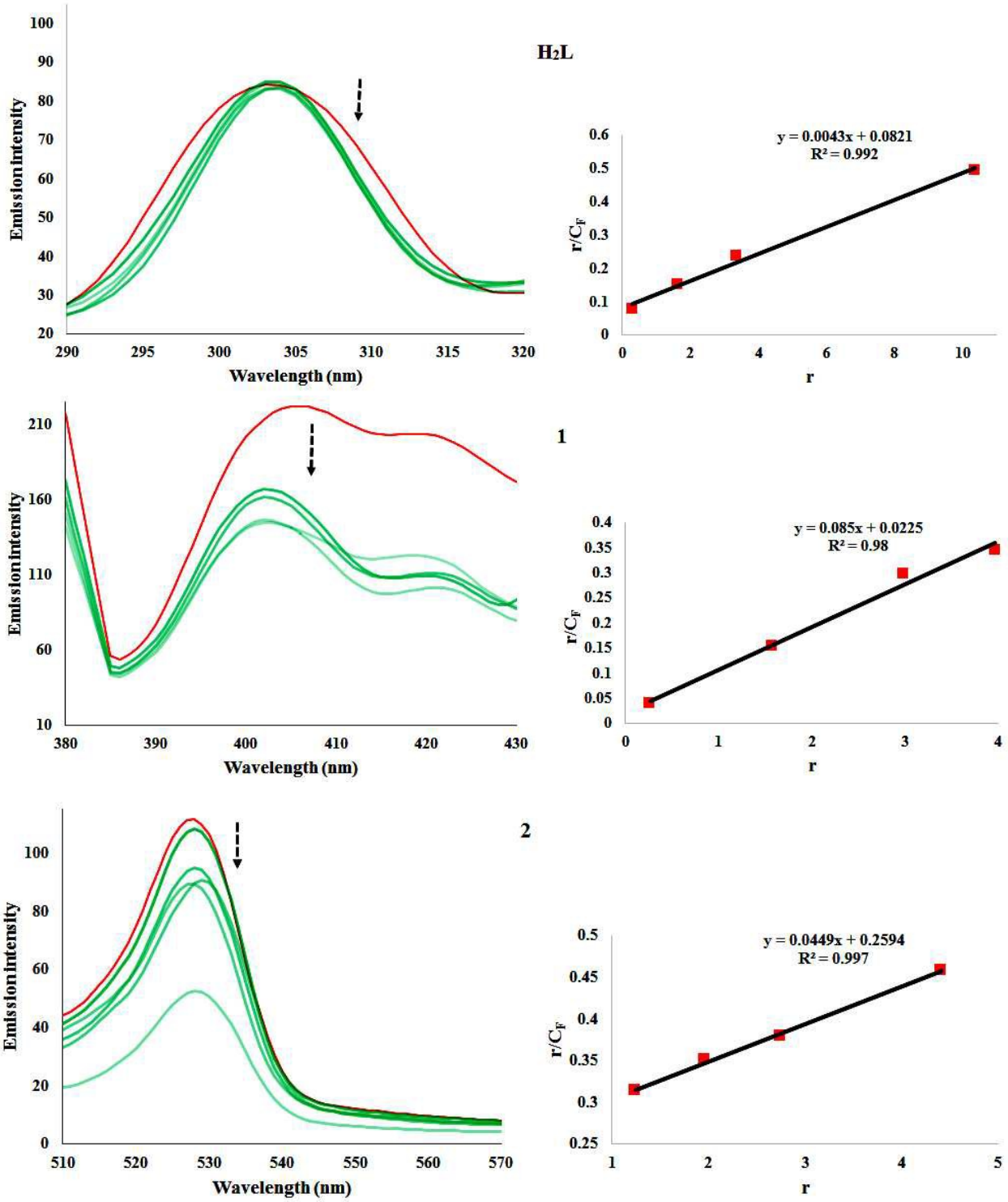

Fig. 5 Fluorescence titrations of **H_2L**, **1** and **2** (25 μM) with CT-DNA (0-50 μM) (left). Scatchard plots of r/Cf *vs* r for selected compounds (right).

Table 5 Fluorescence spectral parameters for compounds **H_2L**, **1** and **2** bound to CT-DNA

Compound	K_b	K_{sv}	K_{app}
H_2L	4.30×10^3	$9.3x10^3$	$8.01x10^3$
1	8.50×10^4	$1.82x10^4$	$3.21x10^5$
2	4.49×10^4	$2.17x10^4$	$3.45x10^5$

From the emissive titration spectra (Fig. 5), it is apparent that upon the addition of increasing concentration of CT-DNA (0-50 μM) to a solution of **H_2L** displayed hypochromism (2.41%) at 304 nm along with small red shift (~2 nm). Complexes **1**, **2** shows different behavior relative to those of the ligand and exhibits the band at 406 and 528 nm showed hypochromism of about 36.36 and 53.27% with a small red shift respectively (~4 nm). The observed hypochromism is due to an intercalative mode of binding involving a strong stacking interaction between extending aromaticity of the ligand and the base pairs of DNA.[35] The binding of compounds to DNA either leads to hypochromism, which provides a measure of the strength of the intercalative. Based on the emission enhancement, the intrinsic binding constant was obtained according to the Scatchard equation:

$$C_b = C_t\,(F - F_0) / F_{max} - F_0)$$

here, C_t is the total compound concentration, F being the observed fluorescence emission intensity at given DNA concentration, F_0 being the intensity in the absence of DNA and F_{max} is the fluorescence of the totally bound compound. The fluorescence spectra of the tested compounds with increasing concentration of CT-DNA are depicted in Fig. 5. Intrinsic binding constant (K_b) were cast in the form of a Scatchard plot of r/C_f versus r, where r is the binding ratio of C_b / [DNA] and C_f is the free ligand concentration. The intrinsic binding constant (K_b) values for the interaction of **H_2L**, **1** and **2** with CT-DNA are listed in Table 5. The binding constant (K_b) of the compounds was in the range of 4.30×10^3 to 8.50×10^4 M^{-1}. However, the complexes interact with CT-DNA more strongly than the ligand. The observed values of K_b revealed that the compounds bind to DNA via intercalative mode, where the order of DNA-binding affinity is **1** > **2** > **H_2L**. However, the binding mode needs to be proved through some more experiments.

Ethidium bromide displacement study

Fluorescence-quenching experiments with EB-bound DNA was undertaken to understand the mode of DNA interaction with the metal complexes. The molecular fluorophore EB emits intense fluorescence at about 600 nm in the presence of DNA due to its strong intercalation between adjacent DNA base pairs.[36] Addition of a second molecule, which bound to DNA more strongly than EB, (actually the fluorescence intensity of EB increases by almost 20-fold after binding to DNA) would displace bound EB and quenched the DNA-induced EB emission. The extent of quenching of the fluorescence of EB bound to DNA would reflect the extent of DNA binding of the second molecule.[37] From the above fact in mind, as the concentration of the **H_2L** and its complexes **1**, **2** increases, the emission band at 604 nm (Fig. 6) for EB exhibited hypochromism up to 26.97, 47.95 and 31.41% with a slight red/blue shift from the initial fluorescence intensity respectively. The quenching of emission intensity of ethidium bromide upon addition of compounds shows that the complexes probably compete with EB for the binding with DNA. Further quantitative assessment of the magnitude of interaction was ascertained by the classical Stern−Volmer equation:

$$I_0/I = 1 + K_{sv}[Q]$$

where I_0 and I are the emission intensities of EB bound CT-DNA in the absence and presence of the quencher (complexes) concentration [Q], respectively, which gave the Stern-Volmer quenching constant (K_{sv}). The K_{sv} value is obtained with a slope from the plot of I_0/I versus [Q] were shown in Fig. 6. The quenching constant (K_{sv}) values were obtained from the slope, thus indicating that the complexes strongly bind to DNA. The quenching constant (K_{sv}) values were obtained from the slope, which were listed in Table 5.

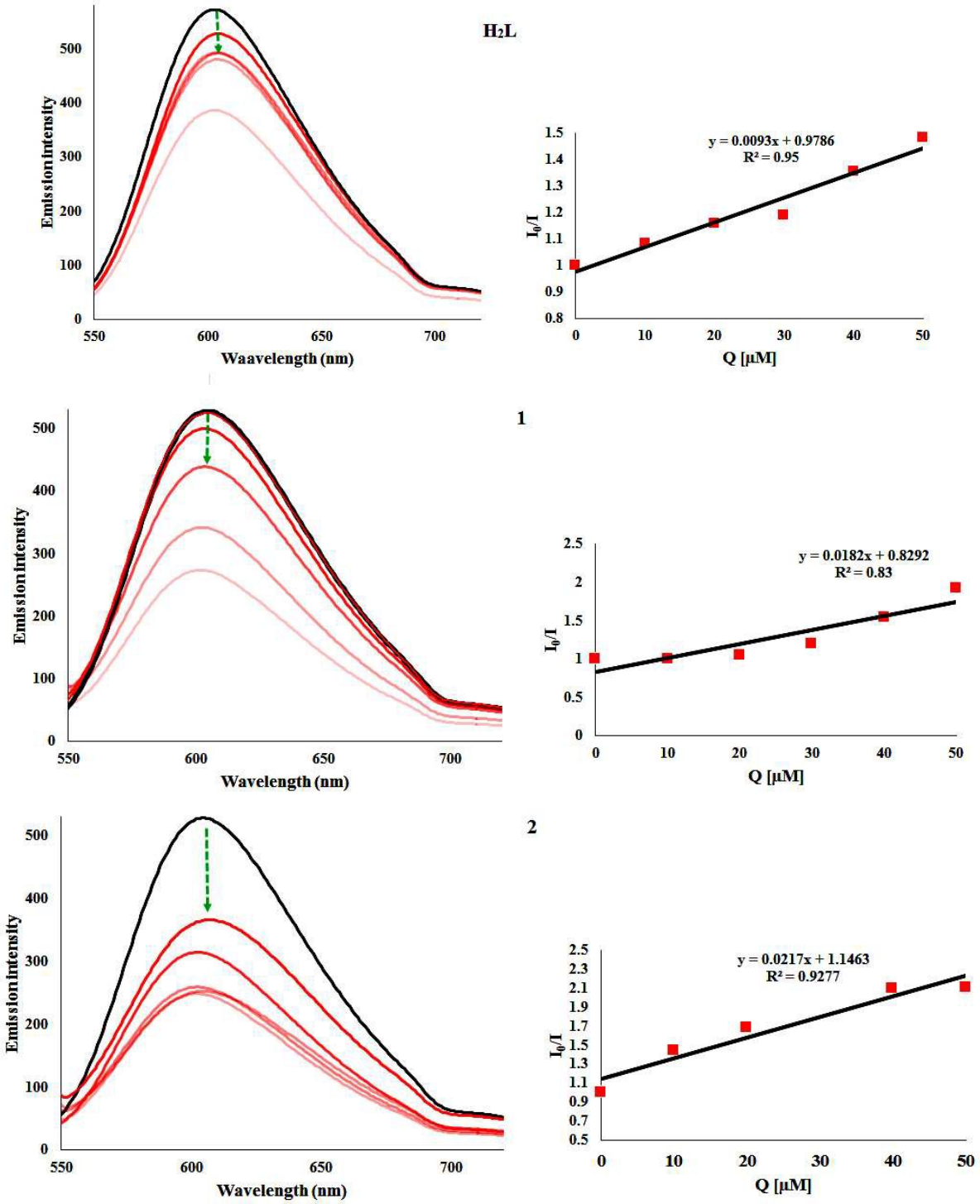

Fig. 6 Fluorescence titrations of **H_2L**, **1** and **2** (0-50 µM) with EB bound CT-DNA (7.5 µM) (left). Scatchard plots of I_o/I *vs* Q for selected compounds (right).

Further the apparent DNA binding constant (K_{app}) values were also calculated using the following equation:

$$K_{EB}\,[EB] = K_{app}\,[M_{50\%}]$$

where $K_{EB} = 1.0 \times 10^{-7}\ M^{-1}$ is the DNA binding constant of EB, [EB] is the concentration of EB (7.5 μM) and $[M_{50\%}]$ is the concentration of the compound used to obtain a 50% reduction in fluorescence intensity of DNA pretreated with EB. The K_{app} value for the ligand and their complexes **1** and **2** were given in Table 5. The DNA binding ability of the compounds follows the order **1** ~ **2** > **H_2L**, which is consistent with the results obtained from the above fluorescence spectral studies.

Viscosity measurement

This technique give us useful information on how the conformation of DNA is influenced by the binding mode of the metal complex to DNA. In general, the viscosity of CT-DNA increases when a compound binds with DNA in intercalating mode but remains unchanged when a compound binds with DNA in electrostatic mode.[38] When the **H_2L** and its complexes **1**, **2** were treated with CT-DNA (200 μM), the concentrations of compounds (0-120 μM) increased from a ratio of R = 0-0.1(1/R = [compound]/[DNA]), the relative viscosity of DNA enlarged steadily in the order **2** > **1** > **H_2L**. The relative viscosity of DNA solution exhibits an increase upon addition of all compounds and it is more pronounced in the case of the complexes (Fig. 7). The observed behavior of the DNA viscosity upon addition of the compounds may be considered evidence of the existence of an intercalative binding mode to DNA, a conclusion which clarifies the preliminary indications derived from fluorescence spectroscopic studies.

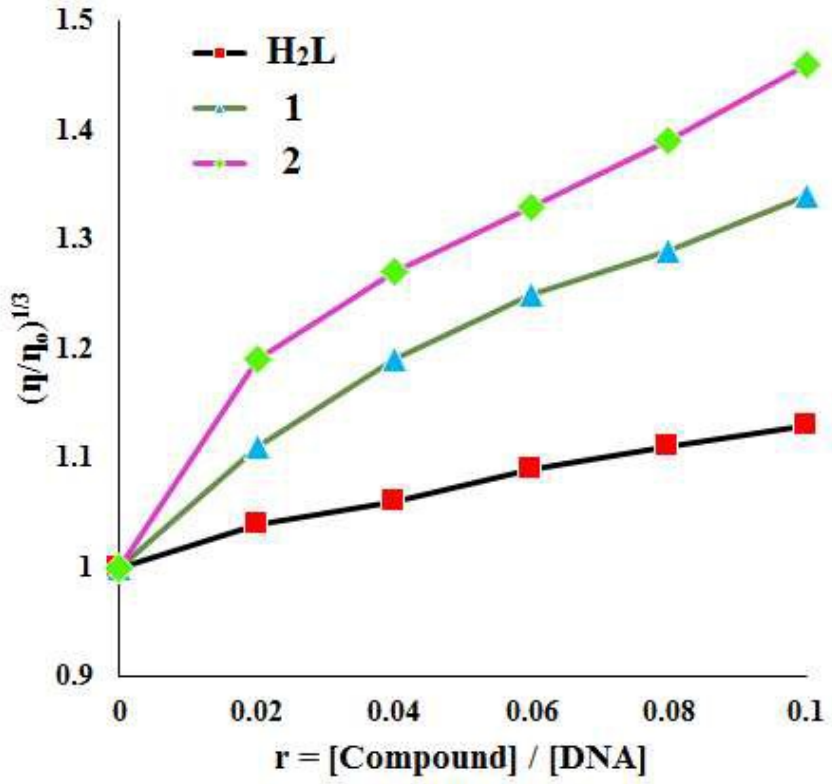

Fig. 7 Relative viscosity $(\eta/\eta_0)^{1/3}$ of CT-DNA in Tris-HCl buffer solution in the presence of tested compounds at increasing amounts (r = 0-0.1).

BSA interaction studies

Fluorescence spectral study

Interaction between the most abundant blood protein, that is, serum albumin, and complexes have attracted immense current interest because of their structural homology with human serum albumin.[39a] To understand the mechanism of interaction between selected compounds and BSA, fluorescence quenching experiments have been carried out. The fluorescence spectra of BSA showed a broad band with a maximum at ~340 nm. The relative ratio of fluorescence intensity for three amino acids and the functions were reported earlier.[33] Therefore, the fluorescence behavior of BSA can provide significant information about the structure, dynamics, and protein folding. A solution of BSA (1 μM) was titrated with various increasing concentrations of the compounds **H_2L**, **1** and **2** (0-50 μM) in the range of wave length

290-430 nm (λ_{ex} = 280 nm). Fig. 8 showed that the effect of increasing concentration of compounds on the fluorescence emission of BSA.

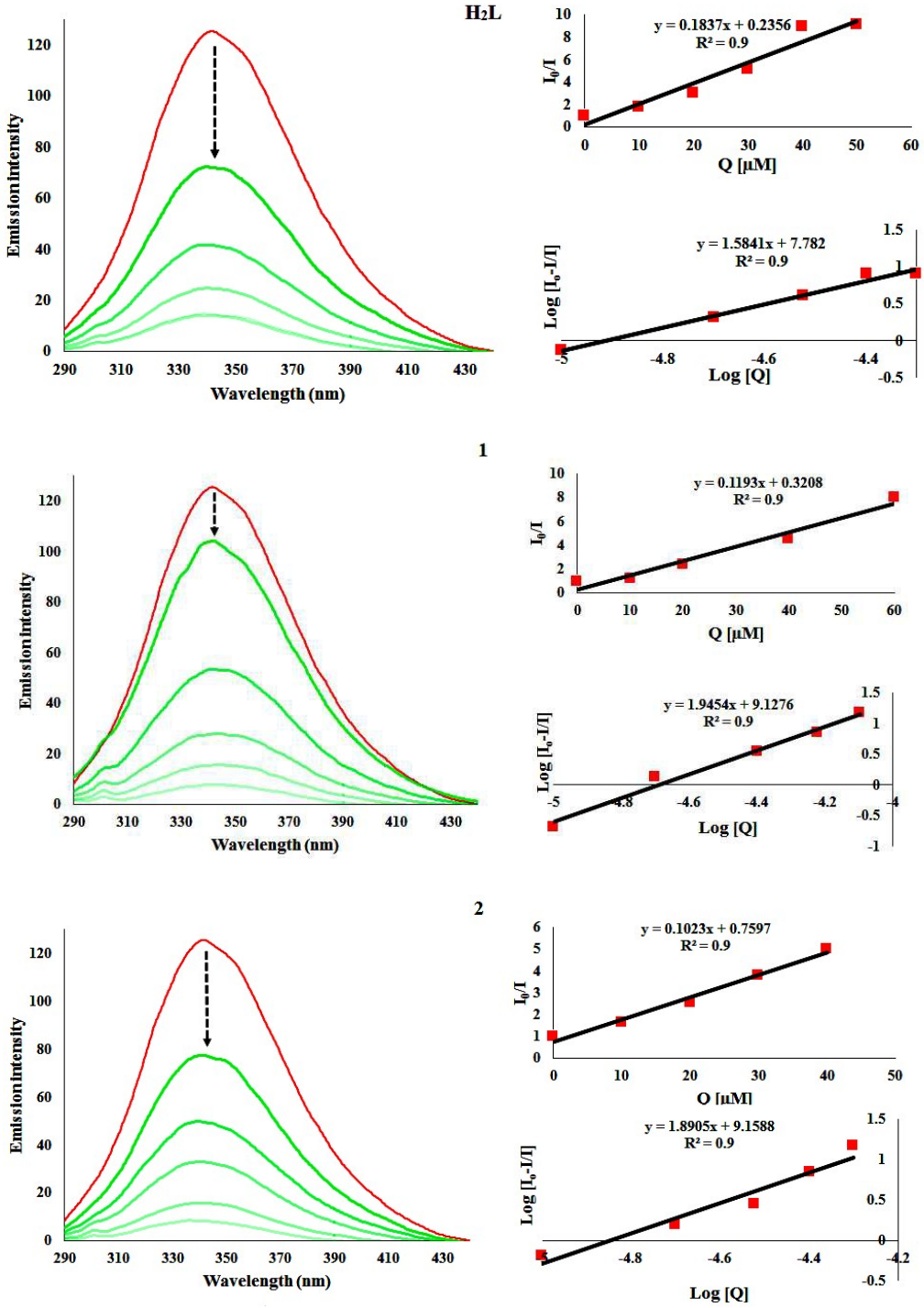

Fig. 8 Fluorescence titrations of **H_2L**, **1** and **2** (0-50 μM) with BSA (1 μM) (left). Stern-Volmer plots of I_o/I *vs* Q and Scatchard plots of Log[Io-I/I] *vs* Log[Q] for selected compounds (right).

Table 6 Quenching parameters of BSA for compounds **H_2L**, **1** and **2**

Compound	K_{sv}	K_q	K_{bin}	'n'
H_2L	$1.83x10^5$	$1.83x10^{13}$	$6.05x10^7$	1.5
1	$1.19x10^5$	$1.19x10^{13}$	$1.34x10^9$	1.9
2	$1.02x10^5$	$1.02x10^{13}$	$1.44x10^9$	1.8

The extent of quenching of fluorescence intensity, as expressed by the value of Stern–Volmer constant (K_{sv}), is a measure of protein binding affinity of the complexes. To have a deep insight into the quenching progression, quenching constant (K_q) was evaluated from following Stern-Volmer equation:

$$I_0/I = 1+ K_{sv}[Q] = 1+ K_q \tau_o [Q]$$

where I_0 and I are the fluorescence intensity in the absence and presence of the quencher, respectively. k_q is the quenching rate constant, τ_o is the fluorescence life time of biopolymer BSA ($\tau_o = 10^{-8}$ s)[39b], K_{sv} and [Q] are the Stern-Volmer quenching constant and the concentration of the quencher respectively. Quenching constant (K_q) have been found from the plot of log (I_0-I) / I *versus* log [Q] (Fig. 8). It can be seen that the K_q value of BSA is higher than 1.0×10^{12}, which is much higher than the molecular fluorescence diffusing constant as shown in Table 6. So the foregoing fluorescence quenching mechanism of the compounds-BSA system cannot be dynamic quenching. It may be static quenching. Nevertheless, the hypothesis needs to be proved through some more experiments.

UV-Visible spectral study

Furthermore it has been proved that the fluorescence quenching mechanism of the compound is static quenching by UV-vis absorption spectral studies. The fluorescence quenching mechanisms are usually classified as either static or dynamic quenching. Static quenching usually results from the formation of a complex between the quencher and the fluorophore in the ground state, whereas in dynamic quenching the fluorophore and the quencher get in touch with each other during the transient existence of the excited state.[40] An effective method to identify the type of quenching was UV-visible absorption spectroscopy. UV-visible spectra of BSA in the

absence and presence of the compounds (Fig. 9) showed that the absorption intensity of BSA was enhanced as the complexes were added, and there was a little blue shift. It revealed that there existed a static interaction between BSA and the added complexes due to the formation of the ground state complex of the type of BSA-compound.

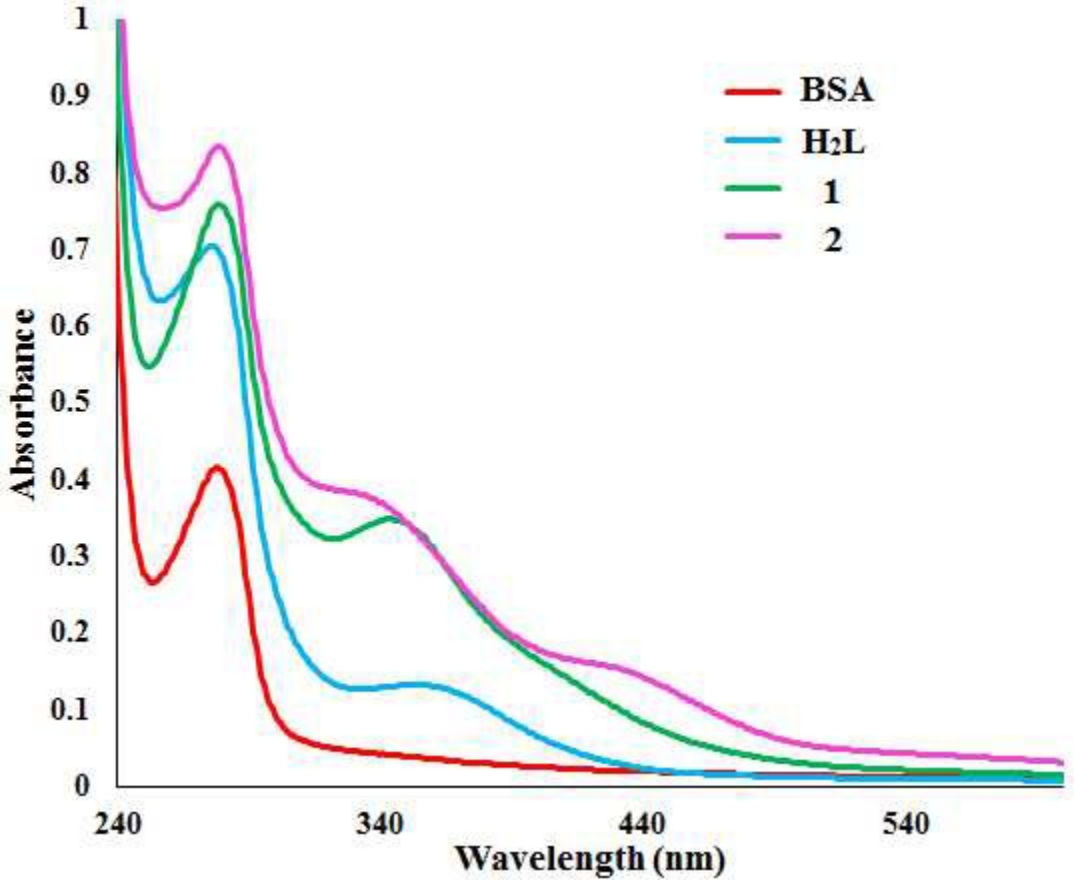

Fig. 9 Absorbance spectra of the compounds **H_2L**, **1** and **2** with BSA.

Binding constant and binding site number

The binding constant K_b was calculated using the Scatchard equation

$$\text{Log } [I_0\text{-}I / I] = \log K_{bin} + n \log [Q]$$

where, K_{bin} is the binding constant of the compound with BSA and 'n' is the number of binding sites. The number of binding sites (n) and the binding constant (K_{bin}) have been found from the plot of log (I_0-I) / I *versus* log [Q] (Fig. 8).[41] The calculated K_{bin}, and n values are given in Table 6. The calculated value of 'n' is around 2 indicating the existence of two binding site available in BSA for all of the compounds. The higher values of K_q and K_{bin} indicates a strong interaction

between the BSA protein and the complexes over the ligand used in this study. It is noticed that the values of binding constant of the compounds follows the order **2** > **1** > **H_2L,** which is consistent with the results obtained from above binding affinity studies.

Catechol oxidase activity

3,5-di-*tert*butylcatechol (3,5-DTBC) was employed as a substrate to study the catalytic performance of the **H_2L** and its complexes **1**, **2** mainly because its low reduction potential makes it easy to oxidize and the bulky *tert*-butyl groups prevent further over oxidation such as ring opening and it is shown a low quinone-catechol reduction potential (Scheme 4).[42] The reactions were carried out at room temperature in aerobic conditions and were monitored by the fluorescence spectroscopic technique. Moreover, the oxidation product of 3,5-di-*tert*butylbenzoquinone (3,5-DTBQ) is highly stable and exhibited a characteristic emission intensity at λ_{emis} = 437 nm (λ_{ex} = 401) in pure DMSO. To monitor the reaction, a 1 × 10^{-4} M solution of selected compounds were treated with 100 equivalents of 3,5-DTBC. Upon the addition of the catecholic substrate, a new band (Fig. 10) was gradually appeared at about 437 nm in time due to the formation of the oxidized product 3,5-DTBQ. Thus, the experiment clearly proves that the oxidation of 3,5-DTBC to 3,5-DTBQ which is catalyzed by the synthesized compounds, as it is well established that 3,5-DTBQ shows a maximum at λ_{emis} = 437 nm in pure DMSO.

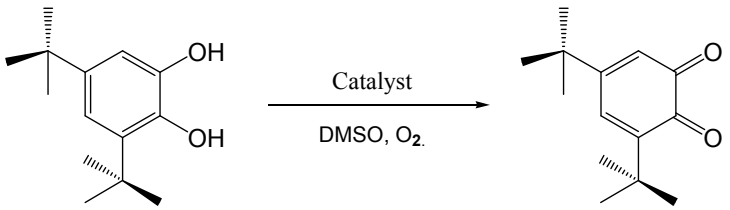

Scheme 4 Catalytic oxidation of 3, 5-DTBC to 3, 5-DTBQ in DMSO in the presence of oxygen.

Kinetic study of the catecholase activity

To understand the kinetic aspects of catalysis for tested compounds, the rate constant for compounds as catalyst was determined by traditional initial rate methods (detailed description provided in the experimental section). The catalytic behavior shows saturation kinetics, and a

treatment based on the Michaelis–Menten model seemed to be appropriate under excess substrate conditions.[43a] The observed rate constants (k_i) were extracted by the initial rate method. Plots of k_i vs. [3,5-DTBC] gave non-linear curve of decreasing slope (Fig. S10) which are best described by the following equations.

$$C + S \underset{k_{-1}}{\overset{k_1}{\rightleftharpoons}} CS \overset{k_2}{\rightleftharpoons}_{k_{-2}} C + P$$

$$V = \frac{V_{max}[S]}{K_M + [S]}$$

$$\frac{1}{V} = \frac{K_M}{V_{max}} \frac{1}{[S]} + \frac{1}{V_{max}}$$

A plausible mechanism for 3,5-DTBC oxidation promoted by metal(II) complexes is schematically depicted in Scheme 5. Unfortunately we were unable to characterize the intermediates. However, when a mixture of starch-potassium iodide solution was added to a mixture of complex and 3, 5-DTBC, blue coloration developed, which indicates that hydrogen peroxide was produced during the course of reaction. It is interesting to note that no blue coloration was observed in absence of 3,5-DTBC. A believable mechanistic path of the formation of H_2O_2 as by-product during the oxidation of 3,5-DTBC to 3,5-DTBQ catalyzed by metal(II) compounds was suggested by Chyn and Urbach.[43b]

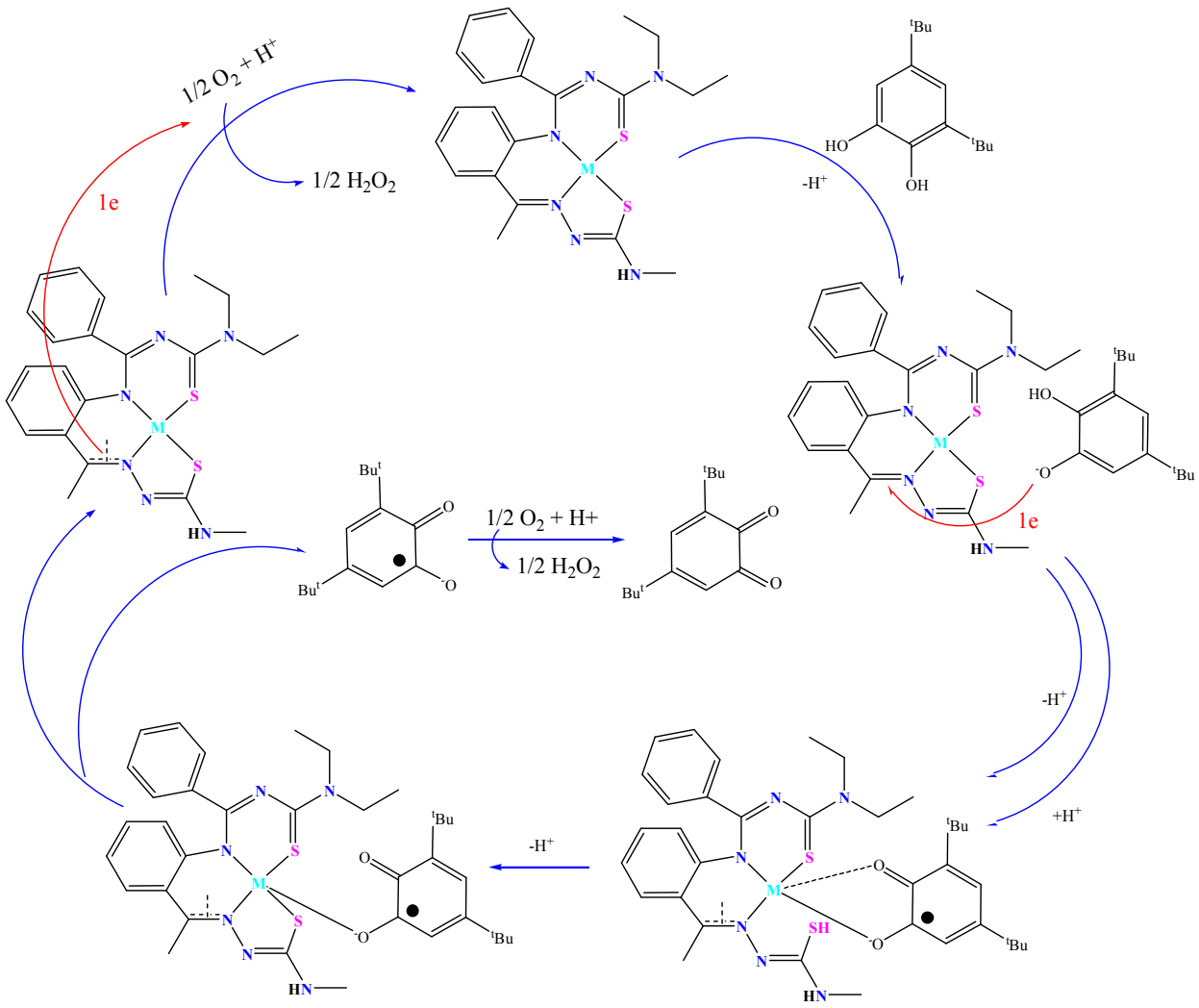

Scheme 5 Plausible mechanism for oxidation of 3,5-DTBC by complexes **1, 2**

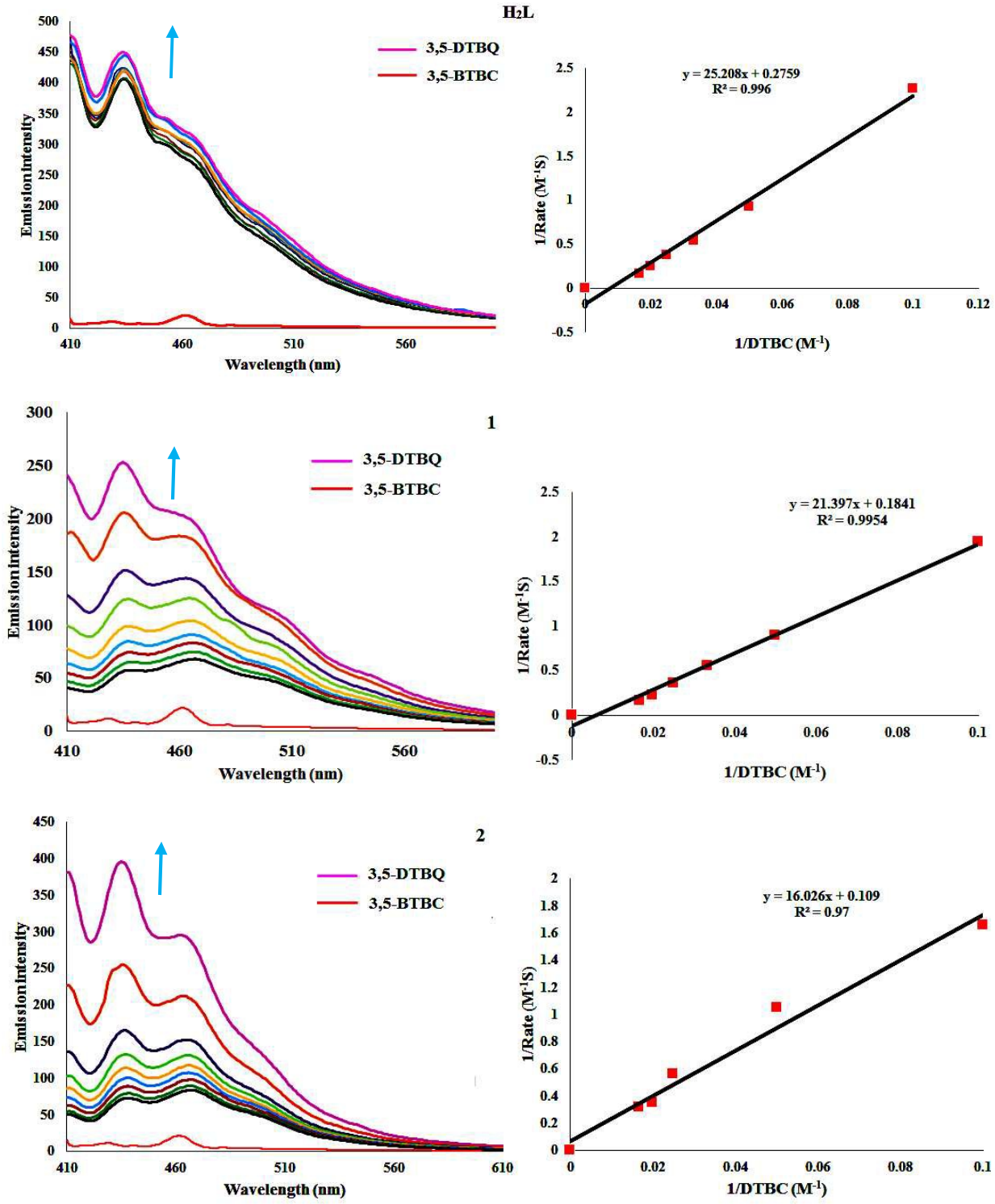

Fig. 10 Oxidation of 3,5-DTBC by **H_2L** and its complexes **1, 2** monitored by flourescence spectroscopy (left). Lineweaver–Burk plot for tested compounds (right).

Table 7 Kinetic parameters for the catecholase activity of **H_2L** and its complexes **1, 2**

Catalyst	K_m (M)	V_{max} (Mm^{-1})	K_{cat} (h^{-1})
H_2L	9.16×10^{-3}	3.64×10^{-4}	91.3
1	1.12×10^{-2}	5.25×10^{-4}	116
2	1.46×10^{-2}	9.17×10^{-4}	146

According to the reported generalized catecholase reaction plausible mechanism (Scheme 5), electron transfer is mainly assisted by metal center and then further delocalized via C=N bond of metal(II) complexes to the adjacent conjugate system. Particularly when chelate formation establishes an extended system of delocalized π-electron density, the probable tautomer of ligand bonding situation showed in Scheme 3. The Michaelis–Menten constant (K_m) and maximum initial rate (V_{max}) were determined by linearization using Lineweaver-Burk plots (Fig. 10). The rate constant for dissociation of substrates S (i.e., turnover number, k_{cat}) were calculated from the graphs of 1/V *vs* 1/[S] (Fig. 10), known as the Lineweaver–Burk graph using the above equation and all these parameters are listed in Table 7. Upon comparison of Table 7, it may be stated that complexes **1** and **2** belong to the highly efficient catalyst group, where the order of their activity is **2** > **1** > **H_2L**.

Phosphate hydrolysis activity

Many metalloenzymes with hydrolytic properties contain metal ions in close proximity to the active site. The selected compounds meet the requisites for use as a functional model system for hydrolytic enzymes. To study the phosphatase activity of compounds, 4-nitrophenyl phosphate disodium salt hexahydrate (4-NPP) (Scheme 6) was the preferred choice of substrate.[44] Its hydrolytic tendency was detected using emissive intensities by monitoring the time evolution of *p*-nitrophenolate ion (4-NP) in DMSO at λ_{emis} = 436 nm (λ_{ex} = 401 nm) through a wavelength scan from 400–800 nm over 2 hour with 40 equivalent of the substrate were used relative to the catalyst.

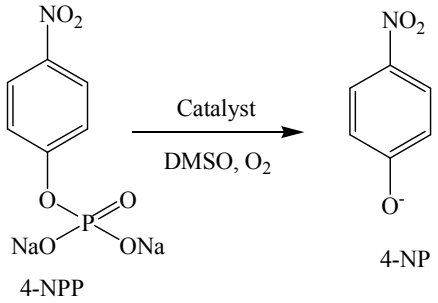

Scheme 6 Catalytic hydrolysis of 4-nitrophenyl phosphate disodium salt hexahydrate (4-NPP) to 4-nitrophenolate ion (4-NP) in DMSO

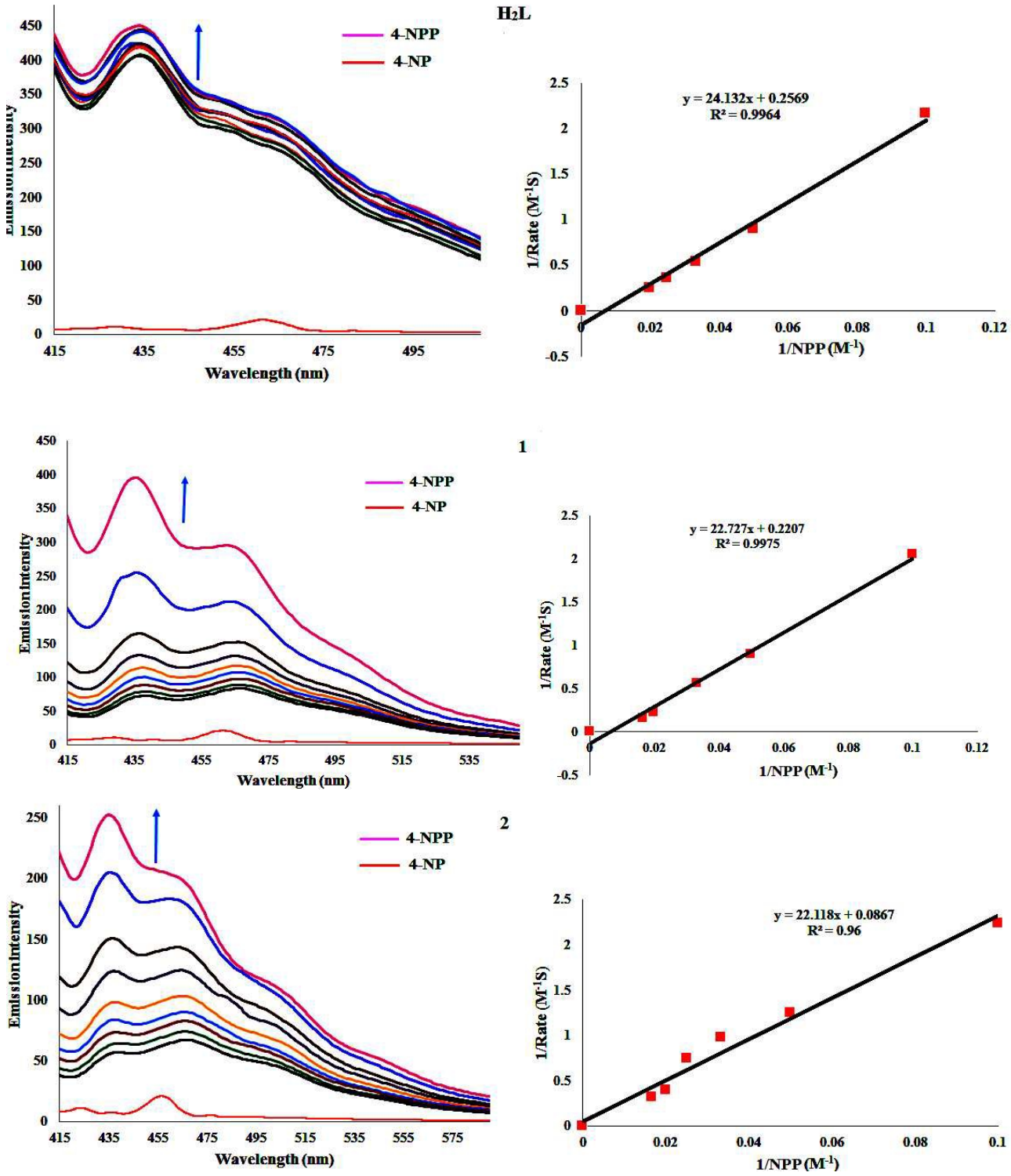

Fig. 11 Hydrolysis of 4-NPP by **H_2L** and its complexes **1, 2** monitored by flourescence spectroscopy (left). Lineweaver–Burk plot for tested compounds (right).

Table 8 Kinetic parameters for the phosphatase activity of **H_2L** and its complexes **1, 2**

Catalyst	K_m (M)	V_{max} (Mm^{-1})	K_{cat} (h^{-1})
H_2L	9.38×10^{-2}	3.89×10^{-3}	1876
1	10.2×10^{-2}	4.53×10^{-3}	2040
2	2.54×10^{-1}	1.15×10^{-2}	5080

Kinetic study of the phosphatase activity

The kinetic study of compounds were done by the initial-slope method by monitoring the rate of the increase in the emissive intensity band at 423 nm, which corresponds to the increase in 4-nitrophenolate concentration.[45] The catalytic behavior shows saturation kinetics, and a treatment based on the Michaelis–Menten model seemed to be appropriate under excess substrate conditions.[46a] The observed rate constants (k_i) were extracted by the initial rate method. Plots of k_i vs. [4-NPP] gave non-linear curve of decreasing slope (Fig. S11) which are best described by same kinetics of catacholase equation. Understandably, the reaction displays first-order kinetics at lower concentration and gradually differs from unity at higher concentration. The Michaelis–Menten constant (K_m) and maximum initial rate (V_{max}) were determined by linearization using Lineweaver-Burk plots (Fig. 11). The rate constant for dissociation of substrates S (i.e., turnover number, kcat) were calculated from the graphs of 1/V vs 1/[S] (Fig. 11), known as the Lineweaver–Burk graph by using the kinetics equation and all these parameters are listed in Table 8. The results indicates first-order rate constant values, which are comparable to the reported values for phosphate bond cleavage.[47] The order of their catalytic activity is **2 > 1 > H_2L**.

Anticancer activity *in vitro*

Inhibition of cancer cell viability (MTT assay)

The antiproliferative activities of the **H_2L** and its complexes **1**, **2** were appraised against normal Vero cell line, human melanoma skin cancer cell line (A375) human cervical cancer (HeLa) and human hepatocellular carcinoma (Hep3B) cancer cell lines using the MTT assay. Cisplatin were used as the reference compounds to evaluate the cytotoxic activity. Cells were exposed to a broad range of drug concentrations (10-100 µg/ml) for 24 h and cell viability was

analyzed by colorimetric MTT assay.[48] The results were analyzed by cell viability curves and expressed with IC_{50} values of the **H_2L** and its complexes **1**, **2** (Table 9). The amount of cell proliferation significantly decreased in a dose-dependent manner on supplementation with the selected compounds (**H_2L**, **1** and **2**), as observed within 24 h of incubation with the normal Vero cancer cell line such as A375, HeLa and Hep3B, because thiosemicarbazones are known inhibitors of enzyme ribonucleotide diphosphate reductase (RDR).[49] RDR is responsible for maintaining a balanced supply of dNTPs required for DNA synthesis and repair and plays an important role in cell proliferation. The ligand **H_2L** was expressed moderate cytotoxicity against normal and cancer cell lines. As can be observed, the results of MTT assays revealed that compounds show notable activity against cancer cell lines (A375, HeLa, Hep3B) with low IC_{50} values. Moreover, when we compare these observations, the coordination of a metal to the ligand increased their cytotoxic activities. Upon confirmation of the excellent cytotoxicity properties, further staining assay were performed to understand their mechanism of action.

Table 9 *In vitro* cytotoxicity of the compounds in normal and cancer cell lines

Compound	IC_{50}(μg/ml)[a]			
	Vero	A375	HeLa	Hep3B
H_2L	72.92±2.67	56.64±1.69	84.14±0.89	64.56±1.24
1	58.92±1.44	26.64±2.37	15.17±2.03	14.47±2.31
2	59.62±1.02	28.88±1.85	12.83±1.65	11.36±1.57
Cisplatin[b]	ND[c]	12.10± 0.6	13.00± 2.01	ND[c]

[a]Fifty percent inhibitory concentration after exposure for 48 h in the MTT assay
[b]Data from Ref. [49, 33]
[c]No data.

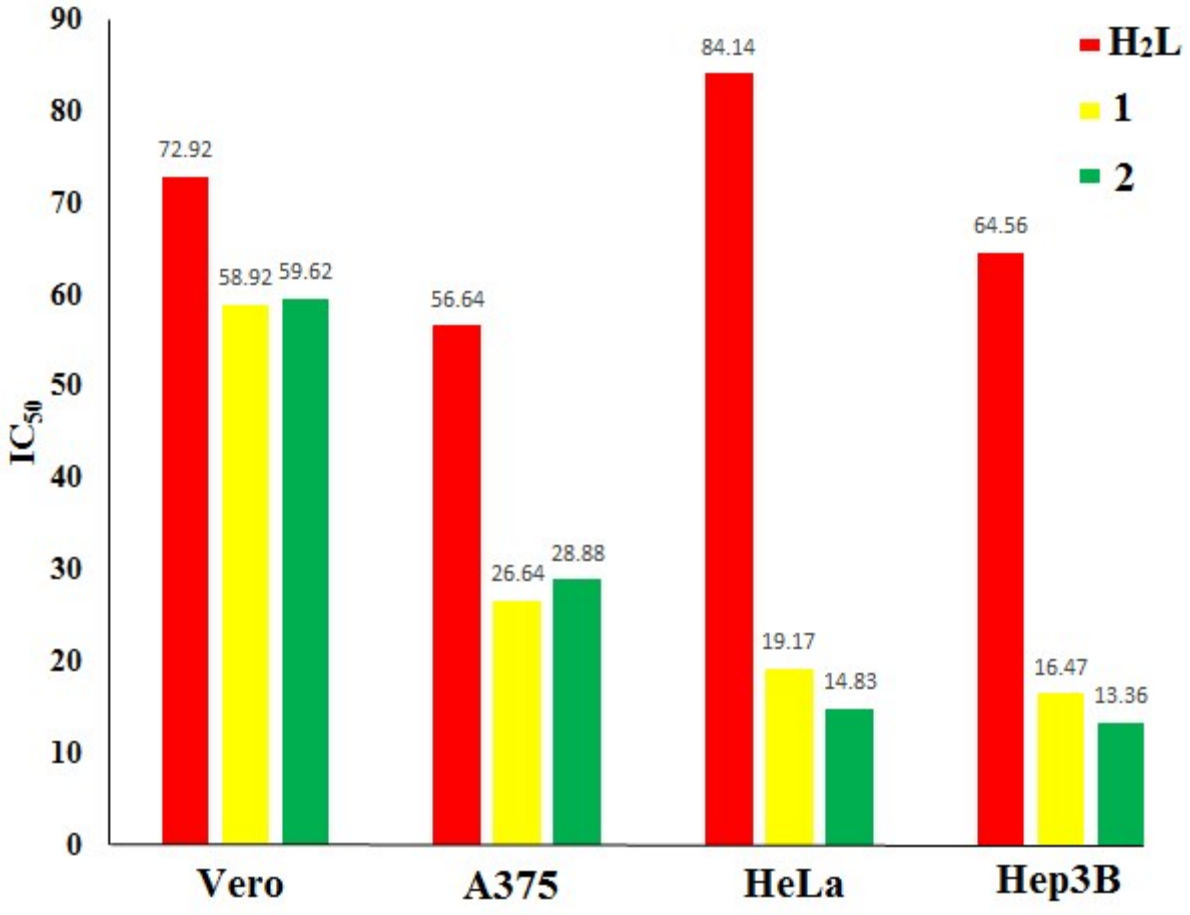

Fig. 12 IC_{50} values of compounds **H_2L**, **1** and **2** on normal Vero and cancer cell lines such as A375, HeLa and Hep3B.

Cell morphological observation for apoptosis induction

To determine the mode of cell death, cells were grown on coverslips, treated with the compounds for 24 h (Fig. 13), and observed for changes in morphology. Apoptosis is the process of programmed cell death (PCD) that may occur in multicellular organisms. These morphological changes include blebbing, cell shrinkage, nuclear fragmentation, chromatin condensation, chromosomal DNA fragmentation and global mRNA decay.[50] So the possible cell death apoptosis in the A375, HeLa and Hep3B cell lines induced by the complex **1** and **2** were primarily studied by the changes observing in the cell morphology after the cells were stained. Apoptotic cells exhibit increased plasma membrane permeability to certain fluorescent dyes, e.g.,

AO/EB, Hoechst, AO/PI, DAPI etc.[51] In this study, we have used membrane-permeable AO/EB and DAPI fluorescence staining.

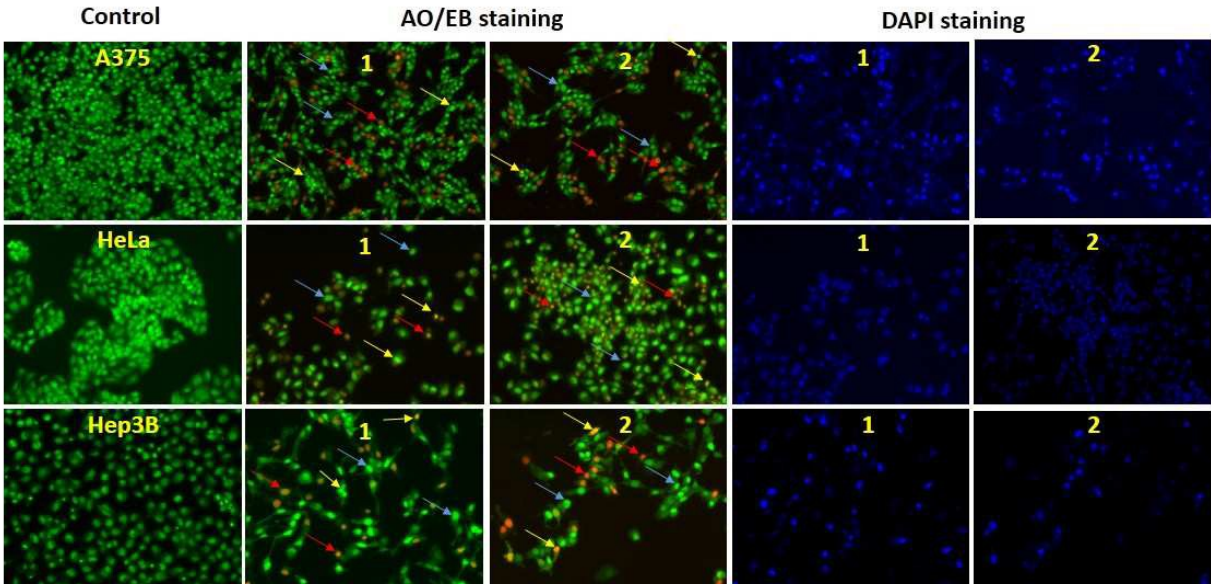

Fig. 13 Images of drug treated A375, HeLa, Hep3B cancer cells after AO/EB and DAPI staining incubated 24 hr treatment of complexes with fixed concentrations. The yellow arrows show early apoptotic cells with blebbing, blue arrows show late apoptosis and red arrows show necrotic cells.

The images of the control cells and treated A375, HeLa and Hep3B cancer cells are depicted in Fig. 13. In this figure yellow arrow(s) showed early apoptotic cells with membrane blebbing which is seen at fixed doses (10 μg/mL) of the complexes and blue arrow(s) exhibited late apoptotic cells with chromatin aggregation that is highly condensed chromatin. The red arrow(s) showed necrotic cells. These are the characteristic features of apoptotic cells and quite different from those of the control cells. Overall the results indicates that complexes favors necrosis at fixed lower dose in good agreement with the reported toxicity results.[52]

Conclusion

Two new metal(II) [M = Ni^{2+} (**1**), Cu^{2+} (**2**)] complexes have been designed and synthesized using doubly deprotonated N_2S_2 hybrid benzamidine-thiosemicarbazone ligand. The characterization of the compounds was accomplished by elemental analyses and various

spectroscopic techniques (IR, UV-vis, ^{1}H NMR) as well as ESI mass spectrometry. The solid state structure of all the compounds was confirmed by single-crystal X-ray crystallography. The geometry of complexes **1** and **2** revealed the square-planer arrangement around the metal ion. On the basis of DFT studies, HOMO-LUMO energy gap explained the eventual charge transfer interactions taking place within the molecule. The lowering of HOMO-LUMO band gap supported bioactive property of the molecule. The structural parameters of the complexes that are in good agreement with X-ray analysis were obtained by DFT calculations. The CT-DNA binding propensities of the compounds were determined by various physico-chemical techniques. All the experimental results showed that the complexes interact with CT-DNA strongly by intercalative binding mode. Furthermore, the results of the fluorescence quenching experiments of BSA concluded that the complexes have binding affinity in static mode. Apart from the above mentioned interaction, the compounds showed effective bio catalytic activity for the oxidation of 3,5-DTBC and the hydrolysis of 4-NPP. The complexes showed widespread anti-tumor potency with low IC_{50} values tested by MTT assay against normal Vero cell line and skin (A375), cervical (HeLa) and liver (Hep3B) cancer cell lines. The characteristics of apoptosis in cell morphology have been observed using AO/EB and DAPI staining. The results attained from the present compounds are of importance for the development of metal-based agents for anti-cancer applications.

Experimental section

Materials

All chemicals used in this study were reagent grade and used without further purification. Solvents were purified and dried according to the standard procedures. All synthetic manipulations were routinely performed under oxygen atmosphere. Doubly distilled water was used to prepare buffers. Calf thymus DNA (CT-DNA), Bovine serum albumin (BSA), 4-nitrophenyl phosphate disodium salt hexahydrate (4-NPP) were obtained from Genei, Bangalore and Himedia, India respectively. Ethidium bromide (EB), 3,5-di-*tert*-butylcatechol (3,5-DTBC), Tris(hydroxymethyl) amino methane were purchased from Sigma-Aldrich and used as received. The synthesis of the N,N-(diethylaminothiocarbonyl)benzimidoyl chloride was performed as multi-step synthesis by the standard procedure of Beyer et al.[10] The reported method was used

for synthesis primary amines such as 2-aminoacetophenone-N^4-methylthiosemicarbazone,[25] except that the purification was carried out by recrystallization from ethanol.

General methods

Elemental analyses (C, H, N and S) were carried out on a Vario EL III CHNS analyzer. Infrared spectra were recorded as KBr pellets using a Perkin-Elmer FT-IR spectrophotometer in the range 4000-400 cm^{-1}. ^{1}H-NMR spectra were measured on a Bruker Ultra Shield at 300 MHz using $CDCl_3$ as solvent and TMS as an internal reference. Mass spectra for the complexes were recorded on an advanced Q-TOF micro™ mass spectrometer using electrospray ionization probe. All MS results are given in the form: m/z, assignment. Electronic spectra have been obtained on a JASCO V-570 spectrophotometer. ESR spectrum was recorded on a JEOL model JES FA_{200} ESR spectrometer at liquid nitrogen temperature operating at X-band frequency (9.45 GHz). Geometry optimization by density functional theory (DFT) method were performed using the B3LYP/6-311G package. Fluorescence spectral data were performed on a JASCO FP-8200 fluorescence spectrophotometer at room temperature. Single crystal X-ray diffraction data collections were carried out at 100(2) K and 295(2) K on a Bruker Apex-II CCD area-detector equipped with a liquid nitrogen cryostat. The melting points were checked on a technico micro heating apparatus and are uncorrected. Stock solutions of compounds (1.0×10^{-3} M in DMSO) were stored at 4^{o}C and required concentrations prepared for all experiments. All the stock solutions used after no more than four days. Solutions of compounds were freshly prepared 1 hour prior to biochemical evaluation. Data were expressed as the mean ± the standard deviation from three independent experiments.

Synthesis of ligand (H_2L)

Solid N-(diethylaminothiocarbonyl)benzimidoyl chloride (1.018 g, 4 mmol) was added to a mixture of 2-aminoacetophenone-N^4-methylthiosemicarbazone (0.889 g, 4 mmol) and triethylamine (1.01 g, 10 mmol) in 10 mL of absolute ethanol. The mixture was stirred for 2 h at 60 °C. The organic solvent was evaporated under reduced pressure to dryness. The residue was dissolved in 20 mL of THF and brine solution (20 mL) was added. The organic layer was separated, dried over $MgSO_4$, filtered, and the solvent was removed in *vacuo*. The residue was

washed with diethyl ether and dried in vacuum to give H_2L as a pure yellow solid. Single crystals suitable for X-ray determination were grown by slow evaporation of an ethanol solution of **H_2L** at room temperature.

Yield: 45% (0.616 mg). Color: Yellowish orange; MP: 170 °C; Micro analytical data for $C_{22}H_{28}N_6S_2$ required: C, 59.97; H, 6.40; N, 19.07; S, 14.55%. Found: C, 59.65; H, 6.22; N, 19.46; S, 14.12%; IR (KBr, cm^{-1}): 3302, 3271, 3236 (NH), 1717, 1686, 1668 (C=N), 838, 781 (C=S). UV-vis [$CHCl_3$, λ_{max}, nm (ε, $dm^3mol^{-1}cm^{-1}$)]: 238 (21202), 280 (14089). ^{1}H NMR (300.13 MHz; $CDCl_3$, ppm): 1.22 (t, J=7.1 Hz, 3H, CH_3), 1.24 (t, J=7.1 Hz, 3H, CH_3), 1.28 (s, 3H, CH_3), 3.20 (s, 3H, NCH_3), 3.91 (q, J=7.1 Hz, 2H, NCH_2), 3.87 (q, J=7.1 Hz, 2H, NCH_2), 7.16 (t, J=7.1 Hz, 2H, Ph), 7.17–7.21 (m, 4H, Ph+C_6H_4), 7.36 (m, 3H, Ph+C_6H_4), 8.10 (s, 1H, NH), 8.47 (s, 1H, NH), 12.72 (s, 1H, NH). ESI-MS (calcd, found, m/z) = 440.63, 441.55 $(M + H)^+$.

Synthesis of complexes 1 and 2

$Ni(OAc)_2{\cdot}4H_2O$ (0.2448 g, 0.001 mole) or $Cu(OAc)_2.4H_2O$ (0.1998 g, 0.001 mole) was dissolved in 20 mL of MeOH:$CHCl_3$ (1:1, v/v) and same mixture solution of H_2L (0.4406 g, 0.001 mole) was added at room temperature. After the solution had been continuously stirred for 30 min, three drops of Et_3N in CH_2Cl_2 (5 mL) was added. The reaction mixture was stirred for 2 h at room temperature. The reaction was monitored by thin-layer chromatography (TLC) using a silica gel on aluminum sheets with a 10/90 mixture of ethyl acetate/petroleum ether as the mobile phase. After completion of reaction, the resulting solution was filtered and the filtrate was left tranquil for the slow evaporation of the mother solvent. After three days black colored big crystals suitable for X-ray diffraction were obtained.

[Ni(L)] (1): Yield: 65%. Color: Dark green; MP: 198 °C; Micro analytical data for $C_{22}H_{26}N_6NiS_2$ required: C, 53.13; H, 5.27; N, 16.90; S, 12.90. Found: C, 53.01; H, 5.35; N, 16.36; S, 12.52%. IR (KBr, cm^{-1}): 3417 (NH), 1715 (C=N), 1527 (C=N), 1601 (C-N), 784 (C=S), 761 (C-S). UV-vis [$CHCl_3$, λ_{max}, nm (ε, $dm^3mol^{-1}cm^{-1}$)]: 236 (13924), 296 (8056), 367 (8132), 431 (7300). ^{1}H NMR (300.13 MHz, $CDCl_3$, ppm): 1.28 (t, J=7.2 Hz, 3H, CH_3), 1.32 (t, J=7.2 Hz, 3H, CH_3), 3.74 (d, J=5.0, 3H, NCH_3), 3.76 (s, 3H, N=C-CH_3), 3.86 (m, 1H, NCH_2), 3.89 (m, 1H, NCH_2), 4.06 (m, 1H, NCH_2), 4.10 (m, 1H, NCH_2), 4.85 (s, br, NH), 6.40 (d, J=8.0

Hz, 1H, C_6H_4), 6.78 (t, J=7.6 Hz, 1H, C_6H_4), 6.85 (t, J=7.7 Hz, 1H, C_6H_4), 7.10 (m, 3H, Ph), 7.27 (d, J=7.2 Hz, 2H, Ph), 7.54 (d, J=7.9 Hz, 1H, C_6H_4). ESI-MS (calcd, found, m/z) = 497.31, 498.42 $(M + H)^+$

[Cu(L)] (2): Yield: 60%. Color: Dark brown; MP: 215 °C; Micro analytical data for $C_{22}H_{26}N_6CuS_2$ required: C, 52.62; H, 5.22; N, 16.74; S, 12.77. Found: C, 53.22; H, 5.05; N, 16.36; S, 12.52%. IR (KBr, cm^{-1}): 3390 (NH), 1700 (C=N), 1547 (C=N), 1572 (C-N), 790 (C=S), 764 (C-S). UV-vis [$CHCl_3$, λ_{max}, nm (ε, $dm^3mol^{-1}cm^{-1}$)]: 237 (13656), 298 (7800), 374 (7912), 491 (8176). ESR (X-band, 9.45 GHz, LNT): $g_{\|}$ 2.078, $g_{\perp}$ 2.031, g_{av} 2.046. ESI-MS (calcd, found, m/z) = 502.06, 503.52 $(M + H)^+$

X-ray structure determination

Suitable single crystals of **H_2L** and its complexes **1**, **2** were mounted on a glass fiber with epoxy cement. The crystals were cut into a fitting size (less than collimator cross section diameter). The crystal data collections were performed with a Bruker SMART APEX 2 at 100(2) (**H_2L**) and a Gemini A Ultra Oxford diffraction diffractometer at 295(2) K (Complex **1, 2**). The crystal data were performed using graphite monochromatized Cu (Kα, λ= 0.71073 Å) for **H_2L** and Mo (Kα, λ= 0.71073 Å) for complexes **1**, **2** throughout. The data were corrected for Lorentz and polarization effects with the SMART14 suite programs and for absorption effects with SADABS.[52] A data collection strategy using ω and φ scans at 0.5° scan technique yielded full hemispherical data with excellent intensity statistics. Structure solutions and refinements were performed using the programs SHELXS-2014.[53] The structures were solved by direct methods to locate the heavy atoms, followed by difference maps for the light non-hydrogen atoms. Anisotropic thermal parameters were refined for the rest of the non-hydrogen atoms. Hydrogen atoms were placed geometrically and refined isotropically. Details of the data collection and refinement are gathered in Table 1 and important bond lengths and angles for the compounds are summarized in Table 2.

Theoretical calculation (DFT)

All calculations were performed using the GAUSSIAN09 (G09) program package with the aid of the Gauss View visualization program. Full geometry optimizations of compounds

were carried out using the DFT method at the Becke's three parameter hybrid exchange functional (B3LYP) level of theory while all the non-metal atoms were described using the 6-311G basis set.[54] This functional has been shown to give more accurate results for all compounds. A difference between the experimental and theoretical datas were carried out the solid and gas phase respectively. Geometry optimizations have been done without any symmetry restriction by X-ray coordinates of the molecule. Frequencies of all complexes have been computed at the same level of theory to confirm all optimized structures are at true minima, which means they have no imaginary frequencies. At the same level and basis sets, calculations of the natural electron population, natural charge for each atom and frontier molecular orbitals of the complexes have been performed by natural bond orbital (NBO) analysis on the gas phase optimized structures.[55] The molecular orbital plots have been generated using the chemcraft program package (http://www.chemcraftprog.com).

DNA–binding studies

Emissive titration

All the experiments concerning the interaction of the complexes with calf thymus (CT) DNA were performed in a mixed solvent of 5% DMSO and 95% Tris-HCl buffer (5 mM Tris-HCl/50 mM NaCl buffer for pH 7.2) for all the experiments and stored at 4 °C for further use. Mixing of such solutions with the aqueous buffer DNA solutions used in the studies never exceeded 5% DMSO (v/v) in the final solution, which was needed due to low aqueous solubility of most compounds. All studies were performed at room temperature. The solvent medium has no influence on the compounds. The CT-DNA concentration per nucleotide was determined by fluorescence spectrometry with a selected compounds wavelength. During titration, an equal quantity of CT-DNA was added to both the complex solution and reference solution to eliminate the intensity of CT-DNA itself and Tris-HCl buffer was subtracted through base line correction. Emissive titration experiments were performed with a fixed concentration of **H_2L** and its complexes **1**, **2** (25 μM). While gradually increasing the concentration (0-10 μM) of DNA, the emission intensities were recorded for selected compounds respect in the range of 300-600 nm. Titrations were manually done by a micropipette for the addition of CT-DNA. It is noteworthy here that the DNA in double distilled water does not show any luminescence.

Ethidium bromide displacement assay

Ethidium bromide displacement assay were carried out by the addition of **H_2L** and its complexes **1**, **2** to sample solution containing EB-DNA. The spectra were recorded at excitation wavelength of 500 nm for an emission range of 605 nm. In the fluorescence quenching spectra, the reduction in emission intensity measures the binding propensity of complex to CT-DNA. This displacement method serves as an indirect evidence to identify intercalative binding modes. EB alone showed minimal fluorescence and the fluorescence was enhanced greatly with gradual addition of CT-DNA until maximum fluorescence was achieved due to the formation of an intercalative DNA-EB adduct. Addition of increasing amounts of the compounds to the DNA-EB adduct quenched the fluorescence. Before the emission spectra were recorded, in these systems CT-DNA was pretreated with EB in the ratio [DNA]/[EB] = 1:1 ratio for 30 minutes at room temperature in order to fully react. Then the titration compounds were added to this mixture of EB-DNA and the change in the fluorescence intensity was measured.

Viscosity experiment

Viscosity measurements were carried out using an Ubbelodhe viscometer maintained at a constant temperature of 30.0°C (± 0.1) in a thermostatic bath. DNA samples of approximately 200 base pairs in length were prepared by sonication in order to minimize complexities arising from CT-DNA flexibility. The flow time was measured three times, after 5 min of incubation, with each addition of the **H_2L** and its complexes **1**, **2** and the average flow time was taken for calculation of relative viscosity. Relative viscosities for CT-DNA in the presence and absence of the compound were calculated from the relation $g = (t - t_o)/t_o$, where t is the observed flow time of DNA-containing solution and t_o is the flow time of Tris–HCl buffer alone. Data were presented as $(\eta/\eta_0)^{1/3}$ versus binding ratio (R = [Compounds] / [DNA] = 0.0-0.1), where η is the viscosity of CT–DNA in the presence of the compound, and η_0 is the viscosity of CT–DNA alone.

Protein binding studies

Quenching of the tryptophan residues of BSA was performed using **H_2L** and its complexes **1**, **2** as quenchers. The fluorescence spectra were recorded at room temperature with an excitation wavelength of BSA at 280 nm and the emission at 344 nm by keeping the

concentration of BSA constant (1 μM) while increasing the complex concentration (0-50 μM) regularly. The excitation and emission slit widths (each 5 nm) remained constant for all the experiments. A scan rate of 500 nm min^{-1} was used. In addition, absorption titration experiments were carried out by keeping the concentration of the complexes (20 μM) and the BSA concentration (1 μM) as constant. Titrations were manually done using a micropipette for the addition of test compounds. The Stern–Volmer and Scatchard equations and graphs may be often used in order to study the interaction of the quencher with BSA.

Kinetic assays

Catechol oxidation

All kinetic experiments were carried out under pseudo-first-order conditions,[56] with **H_2L** and its complexes **1, 2** as the minor component. Quenching of the emission intensity of 3, 5-DTBC at λ_{emis} = 437 nm (λ_{ex} = 401) was monitored using selected compounds. 100 equivalents of 1×10^{-3} M solutions of 3,5-di-*tert*butylcatechol (3,5-DTBC) in DMSO were added to 1×10^{-4} M solutions of selected compounds in DMSO under aerobic conditions. Emissive intensity of the resultant reaction mixture was plotted with respect to wavelength at a regular interval of 15 min in a spectrophotometer in the range of 400 to 700 nm.[7] The dependence of the rate on various concentration and different kinetic parameters were obtained by treatment of a 1×10^{-4} M solution of compounds with 20 to 500 equivalents of substrate and monitoring the upsurge in emission at 437 nm (the peak corresponding to the quinone band maxima) as a function of time.

Phosphate ester hydrolysis

Many metalloenzymes with hydrolytic properties contain metal ions in close proximity to the active site. The selected compound meets the requisites for use as a functional model system for hydrolytic enzymes. The disodium salt of 4-nitrophenylphosphate (4-NPP) was the preferred choice of substrate. Its hydrolytic tendency was detected spectrophotometrically by monitoring the time evolution of *p*-nitrophenolate[57] in DMSO (λ_{max} = 436 nm) through a wavelength scan from 400–600 nm over 2 hour. Quenching of the emission intensity of 4-NPP at 437 nm (excitation wavelength at 401 nm) was monitored using **H_2L** and its complexes **1**, **2**. The hydrolase activities involve the preparation of stock solutions of compounds (0.05×10^{-3} M) and

the substrate 4-NPP (1×10^{-3} M), at higher concentrations in pure DMSO. The dependence of the rate on various concentration and different kinetic parameters were obtained by treatment of a 0.05×10^{-3} M solution of different comounds with 40 equivalents of substrate (the peak corresponding to the phenolate band maxima) as a function of time.

MTT assay

Maintenance of cancer cell lines

The A375 (human malignant melanoma skin cancer), HeLa (human cervical cancer), Hep3B (human hepatocellular carcinoma cancer) cell lines were obtained from National Centre for Cell Sciences Repository, University of Pune, India. Normal Vero and A375, HeLa and Hep3B cancer cells were maintained in a humidified atmosphere containing 5% CO_2 at 37°C in *Dulbecco's modified Eagle's* medium (DMEM) supplemented with 100 units of penicillin, 100 μgmL^{-1} of streptomycin and 10% fetal bovine serum (FBS). Briefly, normal Vero and A375, HeLa, Hep3B cancer cells were precultured in 96-well microtiter plates for 48 h under 5% CO_2.

Preparation of samples for cell line testing

The compounds were dissolved in 0.1% DMSO (the concentration of DMSO did not exceed 0.1% v/v) to obtain a solution of 1 mM each. The samples were then diluted to 100 µM in PBS solution and filter-sterilized using a 0.22 µm syringe filter. This 100 µM solution in PBS was further used in cell cytotoxicity studies. The cells (1×10^6 cells/mL per well) were seeded in a 96-well plate. One day after seeding, the cells were treated with or without different concentration of test compounds and re-incubated at 37 °C in a CO_2 incubator for 24 h. After the incubation, the cells were visualized using an inverted Olympus microscope.

Protocol for MTT assay

The effect of the selected compounds on Vero and A375, HeLa and Hep3B cancer cells line viability were determined by 3-(4,5-dimethylthiazol-2-yl)-2,5-diphenyltetrazolium bromide (MTT) assay. The selected compounds were added to the micro wells containing the cell culture at final concentrations of the range 10-100 µg/mL. Then each well was loaded with 10 µL MTT solution (5 mg mL^{-1} in PBS pH = 7.4) for 4 hour at 37 °C. The purple formazan crystal was

dissolved in 200 μL DMSO and the cell viability was determined by calculating the absorbance of each well at 540 nm using a BIORAD ELISA plate reader.[58] All data were representative of three independent experiments, and the percentage of cell viability was calculated according to the following equation.

Inhibition rate (IR %) = OD (control) - OD Drug treated cells / OD (control) × 100.

The corresponding IC_{50} (concentration of drug that inhibits cell growth by 50%) value was determined by nonlinear regression analysis using Origin 6.0 software.

Fluorescence morphological investigation

Cellular apoptotic morphological changes, which can be detected by AO/EB/ DAPI staining were studied by fluorescence microscopy. The A375, HeLa and Hep3B cancer cells (1×10^6 in number) were cultured in 6 well plates at 37 ^{0}C in an incubator with fixed concentration of the complexes **1** and **2** (50 μM) for 24 h. The cells were harvested and washed with ice-cold phosphate-buffered saline (PBS) and 40 μL of AO/EB solution (1 part of 100 μg/mL of AO in PBS; 1 part of 100 μg/mL of EB in PBS) was added.[59] After staining, the cells were washed with PBS twice, suspended in 200 μL of PBS, and the nuclear morphology were observed under a fluorescence microscope in less than 20 minutes. For DAPI staining, the treated cells were fixed with 80% ethanol at room temperature for 30 min. The fixative was removed and the cells were washed with PBS for 3 times, and then incubated with DAPI (1 μg/mL) for 45 min at room temperature in the dark. Both techniques were used to determine viable cells, early apoptotic cells with blebbing, and necrotic cells. Acridine orange intercalates into the DNA and gives a green fluorescence and thus the viable cells appear with a green nucleus while early apoptotic cells with a condensed or fragmented nuclei. EB is taken up only by the non-viable cells giving a bright orange nucleus of the dead cells overwhelming the acridine orange stain.[60] DAPI dye is effective for fixed-cell staining and quantitation of DNA content. The A375, HeLa and Hep3B cancer cells were mounted on a slide, and the images were observed under a fluorescent microscope in green/blue filter with excitation at 350 nm and emission at 460 nm. At least 200 cells from each slide were counted, and the percentage of apoptotic cells was calculated on the basis of cellular morphological features. The results were shown as the mean of the three independent experiments.

Acknowledgments

The authors Dr. P.V. and P.V gratefully acknowledge UGC [F.No.40-66/2011 (SR)] for financial support. The author R.N thankful to DST for financial assistance (Project No.SR/FT/CS-95/2010). The authors would like to thank The Director, CAS in Botany, School of Life Sciences, University of Madras, Chennai for providing laboratory facilities to perform the cell lines studies.

Electronic supplementary information (ESI) available:

^{1}H spectra of compounds (Fig. S1, S2), UV-vis spectra of compounds (Fig. S3), EPR spectrum of complex **2** (Fig. S4), Mass spectra of compounds (Fig. S5-S7), π-π stacking interaction of ligand **(**Fig. S8**),** Molecular packing diagram (Fig. S9), Plot for rate *vs* concentration of catacholase activity (Fig. S10), Plot for rate *vs* concentration of phosphatase activity (Fig. S11). CCDC reference numbers 1418962, 1418963 and 1418964 for compounds. For ESI and crystallographic data in CIF or other electronic format see DOI:

References

1. T. W. Hayton and G. J. Wu, *J. Am. Chem. Soc.* 2008, **130**, 2005-2014.
2. M. R. MacDonald, M. E. Fieser, J. E. Bates, J. W. Ziller, F. Furche and W. J. Evans, *J. Am. Chem. Soc.* 2013, **135**, 13310-13313.
3. (a) I. S. R. Karmel, N. Fridman, M. Tamm and M. S. Eisen, *J. Am. Chem. Soc.* 2014, **136**, 17180-17192. (b) C. Camp, J. Pecaut and M. Mazzanti, *J. Am. Chem. Soc.* 2013, **135**, 12101-12111.
4. G. Nocton, J. Pecaut and M. Mazzanti, *Angew. Chem., Int. Ed.* 2008, **47**, 3040-3042.
5. (a) F. Innocenti and M. J. Ratain, *Eur. J. Cancer* 2002, **38**, 639-644. (b) W. Lee, A. C. Lockhart, R. B. Kim and M. L. Rothenberg, *Oncologist* 2005, **10**, 104-111.
6. S. H. V. Rijt, and P. J. Sadler, *Drug Discov. Today* 2009, **14**, 1089-1097.
7. J. S. Casas, M. S. García-Tasende and J. Sordo, *Coord. Chem. Rev.,* 2000, **209**, 197-261.
8. D. X. West, A. E. Liberta, S. B. Padhye, R. C. Chikate, P. B. Sonawane, A. S. Kumbhar and R. G. Xerande, *Coord. Chem. Rev*., 1993, **123**, 49–71.
9. A. R. Cowley, J. R. Dilworth, P. S. Donnelly, E. Labisbal and A. Sousa, *J. Am. Chem. Soc.*, 2002, **124**, 5270–5271.
10. (a) L. Beyer and R. Widera, *Tetrahedron Lett.* 1982, ***23***, 1881-1882. (b) L. Beyer, J. Hartung and R. Widera, *Tetrahedron* 1984, **40**, 405-412.
11. M. Christlieb and J. Dilworth, *Chem. Eur. J*. 2006, **12**, 6194-6206.
12. R. Ramachandran, G. Prakash, S. Selvamurugan, P. Viswanathamurthi, J. G. Malecki and V. Ramkumar, Dalton Trans., 2014, **43**, 7889–7902.
13. R. Manikandan, N. Chitrapriya, Y. J. Jang and P. Viswanathamurthi, RSC Adv., 2013, **3**, 11647-11657.
14. P. Anitha, N. Chitrapriya, Y. J. Jang and P. Viswanathamurthi, *J. Photochem. Photobiol. B.,* 2013, **129**, 17-26.
15. a) P. Vijayan, P. Viswanathamurthi, V. Silambarasan, D. Velmurugan, K. Velmurugan, R. Nandhakumar, R. J. Butcher, T. Silambarasan and R. Dhandapani, *J. Organomet. Chem.,* 2014, **768**, 163-177. (b) A. Winter, K. Thiel, A. Zabel, T. Klamroth, A. Poppl, A. Kelling, U. Schilde, A. Tauberta and P. Strauch, New J. Chem., 2014, 38, 1019-1030.

16. F. Arnesano, M. Losacco and G. Natile, *Eur. J. Inorg. Chem*., 2013, **15**, 2701–2711.

17. J. D. Hoeschele, *Dalton Trans.,* 2009, **38**, 10648–10650.

18. J. Reedijk, *Eur. J. Inorg. Chem.,* 2009, **10**, 1303–1312.

19. a) K. Das, A. Datta, P-H. Liu, J-H. Huang, C-L. Hsu, W-T. Chang, B. Machura and C. Sinha, *Polyhedron,* 2014, 71, 85-90. (b) E. Zangrando, M. T. Islamb, M. Al-Amin A. A. Islam, M. C. Sheikh, M. T. H. Tarafder, R. Miyatake, R. Zahanf and M. A. Hossain, *Inorg. Chim. Acta.,* 2015, 427, 278-284. (c) S. Anbu, S. Kamalraj, A. Paul, C. Jayabaskaran and A. J. L. Pombeiro, Dalton Trans.,2015, 44, 3930-3933. (d) V. S. Li, D. Choi, Z. Wang, L. S. Jimenez, M. S. Tang and H. Kohn, *J. Am. Chem. Soc*., 1996, **18**, 2326–2331.

20. J. C. Venter, M. D. Adams, E. W. Myers and P. W. Li, *Science*, 2001, **291**, 1304-1351.

21. a) R. Loganathan, S. Ramakrishnan, E. Suresh, A. Riyasdeen, M. A. Akbarsha and M. Palaniandavar, *Inorg. Chem.,* 2012, **51**, 5512-5532. (b) R. P. Paitandi, R. K. Gupta, R. S. Singh, G. Sharma, B. Koch and D. S. Pandey, *Eur. J. Med. Chem.,* 2014, 84, 17-29.

22. P. Jaividhya, R. Dhivya, M. A. Akbarsha and M. Palaniandavar, *J. Inorg. Biochem.,* 2012, **114**, 94-105.

23. W. Hong, H. Lee, T. H. Noh and O.-S. Jung, Dalton Trans. 2013, **42**, 11092–11099.

24. a) R. Sanyal, A. Guha, T. Ghosh, T. K. Mondal, E. Zangrando and D. Das, *Inorg. Chem.* 2014, **53**, 85–96. (b) M. Mitra, P. Raghavaiah and R. Ghosh, *New J. Chem.,* 2015, 39, 200-205. (c) M. Pait, M. Shatruk and D. Ray, *Dalton Trans*., 2015, 44, 11741-11754.

25. D. X. West, A. A. Nassar, F. A. E. l. Saied and M. I. Ayad, *Trans. Met. Chem*. 1999, **24** 617-621.

26. H. H. Nguyen and U. Abram, *Eur. J. Inorg. Chem.* 2009, **21**, 3179-3187.

27. H.H. Nguyen, J. Grewe, J. Schroer, B. Kuhn and U. Abram, *Inorg. Chem.* 2008, **47,** 5136-5144.

28. H. H. Nguyen and U. Abram, *Polyhedron*, 2009, **28**, 3945-3952.

29. A. Barandov and U. Abram, *Inorg. Chem*. 2009, **48**, 8072-8074.

30. J. Schroer and U. Abram, *Inorg. Chem. Commun.* 2010, **13**, 26-29.

31. a) R. Prabhakaran, P. Kalaivani, S. V. Renukadevi, R. Huang, K. Senthilkumar, R. Karvembu and K. Natarajan, *Inorg. Chem.,* 2012, **51**, 3525–3532. (b) R. Prabhakaran, P.

Kalaivani, R. Huang, P. Poornima, V. Vijaya Padma, F. Dallemer and K. Natarajan, *J. Biol. Inorg. Chem.,* 2013, 18, 233-247.

32. R. Bauernschmitt and R. Ahlrichs, *Chem. Phys. Lett*., 1996, **256**, 454–464.
33. P. Vijayan, P. Viswanathamurthi, P. Sugumar, M. N. Ponnuswamy, M. D. Balakumaran, P. T. Kalaichelvan, K. Velmurugan, R. Nandhakumar and R. J. Butcher, Inorg. Chem. Front., 2015, **2**, 620-639.
34. Q. Yu, Y. Liu, J. Zhang, F. Yang, D. Sun, D. Liu, Y. Zhou and J. Liu, *Metallomics,* 2013, **5**, 222–231.
35. A. K. Patra, T. Bhowmick, S. Ramakumar, M. Nethaji and A. R. Chakravarty, *Dalton Trans.,* 2008, **28**, 6966-6976.
36. F. J. M. Almes and D. Porschke, *Biochemistry,* 1993, **32**, 4246-4253.
37. M. Alagesan, N. S. P. Bhuvanesh and N. Dharmaraj, *Eur. J. Med. Chem.,* 2014, **78**, 281–293.
38. Y. J. Liu, Z. H. Liang, Z. Z. Li, J. H. Yao and H. L. Huang, *J. Organomet. Chem.* 2011, **696**, 2728-2735.
39. (a) U. K. Laemmli, *Nature*, 1970, **227**, 680–685. (b) J. R. Lackowicz and G. Weber, Biochem. J., 1973, **12**, 4161–4170.
40. Y. J. Hu, Y. Ou-Yang, C.M. Dai, Y. Liu and X. H. Xiao, *Biomacromolecules*, 2010, **11**, 106-112.
41. S. Anbu, R. Ravishankaran, A. A. Karande and M. Kandaswamy. *Dalton Trans.* 2012, **41**, 12970-12983.
42. M. U. Triller, D. Pursche, W. Y. Hsieh, V. L. Pecoraro, A. Rompel and B. Krebs, *Inorg. Chem.,* 2003, **42**, 6274-6283.
43. (a) E. I. Solomon, U. M. Sundaram and T. E. Machonkin, *Chem. Rev.,* 1996, **96**, 2563-2605. (b) J.P. Chyn and F. L.Urbach, *Inorg. Chim. Acta*, 1991, **189**, 157-163.
44. T. Gajda, Y. Düpre, I. Török, J. Harmer, A. Schweiger, J. Sander, D. Kuppert and K. Hegetschweiler, *Inorg. Chem.* 2001, **40**, 4918-4927.
45. S. C. Batista, A. Neves, A. J. Bortoluzzi, I. Vencato, R. A. Peralta, B. Szpoganicz, V.V. E. Aires, H. Terenzi and P. C. Severino, *Inorg. Chem. Commun.,* 2003, **6**, 1161–1165.

46. R. Sanyal, A. Guha, T. Ghosh, T. K. Mondal, E. Zangrando and D. Das, *Inorg. Chem.* 2014, **53**, 85–96.
47. S. E. Bunn, C. T. Liu, Z. L. Lu, A. A. Neverov and S. R. Brown, *J. Am. Chem. Soc*. 2007, **129**, 16238–16248.
48. T. Mosmann, *J. Immunol. Methods,* 1983, **65**, 55-63.
49. X. Q. Zhou, Q Sun, L. Jiang, S. Tong Li, W. Gu, J. L. Tian, X Liu and S. P. Yan, Dalton Trans., 2015, **44**, 9516–9527.
50. S. S. Bhat, A. S. Kumbhar, A. A. Kumbhar and A. Khan, *Chem. Eur. J.*, 2012, **18**, 16383–16392.
51. S. Mukhopadhyay, P. K. Panda, D. N. Das, N. Sinha, B. Behera, T. K. Maiti and S. K. Bhutia, *Acta Pharmacol. Sin.,* 2014, **35**, 814-824.
52. SMART & SAINT *Software Reference manuals*, version 5.0, *Bruker AXS Inc*., Madison, WI, 1998.
53. G. M. Sheldrick, SHELXL97, *Program for Crystal Structure Refinement*, University of Gottingen, Germany, 1997.
54. M. J. Frisch, G. W. Trucks, H. B. Schlegel, G. E. Scuseria, M. A. Robb, J. R. Cheeseman, G. Scalmani, V. Barone, B. Mennucci, G. A. Petersson, H. Nakatsuji, M. Caricato, X. Li, H. P. Hratchian, A. F. Izmaylov, J. Bloino, G. Zheng, J. L. Sonnenberg, M. Hada, M. Ehara, K. Toyota, R. Fukuda, J. Hasegawa, M. Ishida, T. Nakajima, Y. Honda, O. Kitao, H. Nakai, T. Vreven, J. A. Montgomery, J. E. Peralta, F. Ogliaro, M. Bearpark, J. J. Heyd, E. Brothers, K. N. Kudin, V. N. Staroverov, T. Keith, R. Kobayashi, J. Normand, K. Raghavachari, A. Rendell, J. C. Burant, S. S. Iyengar, J. Tomasi, M. Cossi, N. Rega, J. M. Millam, M. Klene, J. E. Knox, J. B. Cross, V. Bakken, C. Adamo, J. Jaramillo, R. Gomperts, R. E. Stratmann, O. Yazyev, A. J. Austin, R. Cammi, C. Pomelli, J. W. Ochterski, R. L. Martin, K. Morokuma, V. G. Zakrzewski, G. A. Voth, P. Salvador, J. J. Dannenberg, S. Dapprich, A. D. Daniels, O. Farkas, J. B. Foresman, J. V. Ortiz, J. Cioslowski and D. J. Fox, *Gaussian 09, Inc.,* Wallingford, CT, 2009.
55. E. Reed, L. A. Curtiss and F. Weinhold, *Chem. Rev.,* 1988, **88**, 899–926.
56. P. Kar, R. Haldar, C. J. Gómez-García and A. Ghosh, *Inorg. Chem.,* 2012, **51**, 4265-4273.

57. J. G. Zalatan and D. Herschlag, *J. Am. Chem. Soc.* 2006, **128**, 1293-1303.
58. A. Husain, X. J. Yan, N. Rosales, C. Aghajanian, G. K. Schwartz and D. R. Spriggs, *Clin. Cancer Res.,* 1997, **3**, 2089–2097.
59. S. Ramakrishnan, V. Rajendiran, M. Palaniandavar, V. S. Periasamy, B. S. Srinag, H. Krishnamurthy and M. A. Akbarsha, *Inorg. Chem*., 2009, **48**, 1309–1322.
60. I. M. Ghobrial, T. E. Witzig and A. A. Adjei, *Cancer J. Clin.,* 2005, **55**, 178-194.

Graphical abstract for:

Nickel(II) and copper(II) complexes constructed with N_2S_2 hybrid benzamidine-thiosemicarbazone ligand: Synthesis, X-ray crystal structure, DFT, kinetico-catalytic and *in vitro* biological applications

Paranthaman Vijayan,[a] Periasamy Viswanathamurthi,*[a] Krishnaswamy Velmurugan,[b] Raju Nandhakumar,[b] Manickam Dakshinamoorthi Balakumaran,[c] Pudupalayam Thangavelu Kalaichelvan,[c] Jan Grzegorz Malecki[d]

[a]*Department of Chemistry, Periyar University, Salem-636 011, India.*

[b]*Department of Chemistry, Karunya University, Karunya Nagar, Coimbatore - 641 114, India.*

[c]*Centre for Advanced Studies in Botany, School of Life Sciences, University of Madras, Guindy Campus, Chennai - 600 025, Tamil Nadu, India.*

[d]*Department of Crystallography, Silsian University, Szkolna 9, 40-006 Katowice, Poland*

We report the nickel(II) and copper(II) complexes containing benzamidine-thiosemicarbazone ligand together with DFT, catalytic and biological applications such as catacholase/phosphatase activities, DNA/BSA affinities and *in vitro* anticancer properties.